



Laser-arc hybrid welding of 12- and 15-mm thick structural steel

Ivan Bunaziv¹ · Cato Dørum² · Steen Erik Nielsen³ · Pasi Suikkanen⁴ · Xiaobo Ren¹ · Bård Nyhus¹ · Magnus Eriksson¹ · Odd M. Akselsen¹

Received: 3 November 2019 / Accepted: 9 March 2020 / Published online: 25 March 2020
© The Author(s) 2020

Abstract

High-power lasers are very effective in welding of plates thicker than 10 mm due to the keyhole mode. High-power intensity generates a vapor-filled cavity which provides substantial penetration depth. Due to the narrow and deep weld geometry, there is susceptibility to high hardness and weld defects. Imperfections occur due to keyhole instability. A 16-kW disk laser was used for single-pass welding of 12- to 15-mm thick plates in a butt joint configuration. Root humping was the main imperfection and persisted within a wide range of process parameters. Added arc source to the laser beam process may cause increased root humping and sagging due to accelerated melt flow. Humping was mitigated by balancing certain arc and other process parameters. It was also found that lower welding speeds (< 1.2 m/min) combined with lower laser beam power (< 13 kW) can be more positive for suppression of humping. Machined edges provided more consistent root quality and integrity compared with plasma cut welded specimens. Higher heat input (> 0.80 kJ/mm) welds provided hardness level below 325 HV. The welded joints had good Charpy toughness at – 50 °C (> 50 J) and high tensile strength.

Keywords Laser welding · Hybrid welding · High strength steel · Thick steel · Mechanical properties · Toughness

1 Introduction

Laser beam welding (LBW) and laser-arc hybrid welding (LAHW) are promising joining methods for a wide variety of industries with extensive range of plate thicknesses from 0.7 up to 50 mm [1]. Thin plates have been successfully joined by laser beam for many decades, primarily in the automotive industry. However, applications of sections with thicknesses > 10 mm have limited use due to high tendency for imperfections and high hardness [2–5]. In the case of fiber/disk lasers (1030–1070 nm wavelength), there are not many studies have been made for such thick plates. When compared with LBW, LAHW is a more advanced process due to the added arc

source. It provides moderate cooling rate which can suppress high hardness [6], and the added filler wire can assist in developing more favorable microstructure [4]. Moreover, LAHW possesses better gap bridgeability and is more tolerant to misalignment [7] which is typical in a real manufacturing case. However, LAHW generates slightly higher residual stresses and distortions than LBW [8]. Therefore, the heat input should be more strictly controlled.

Single-pass welding of thick steel sections may be highly relevant for structural applications. The process is very effective without the need to turn the sections and where access is limited, example is orbital pipeline welding. However, full penetration single-pass welding technique causes specific and serious welding imperfections such as root humping or sagging related to melt dropout. This is a challenge when no backing is allowed. Moreover, backing systems for laser beam welding are not well developed and not readily available in the market. Haug et al. [9] studied the effect of laser power and welding speed on root formation in welding of 12-mm thick steel with two types of laser sources, 1030-nm wavelength (disk laser) and 10,600-nm wavelength (CO₂ laser). It was found that 1030-μm wavelength lasers have very narrow process window due to higher absorption coefficient and subsequent melt overheat in welding of carbon steels. Based on

✉ Ivan Bunaziv
ivan.bunaziv@sintef.no

¹ SINTEF Industry, P.O. Box 4760, Torgarden,
NO-7465 Trondheim, Norway

² Norwegian Public Roads Administration, Bridge Section,
Hamar, Norway

³ FORCE Technology, Park Allé 345, DK-2605 Brøndby, Denmark

⁴ SSAB Europe Oy, Rautaruukintie 155, FI-92100 Raahe, Finland

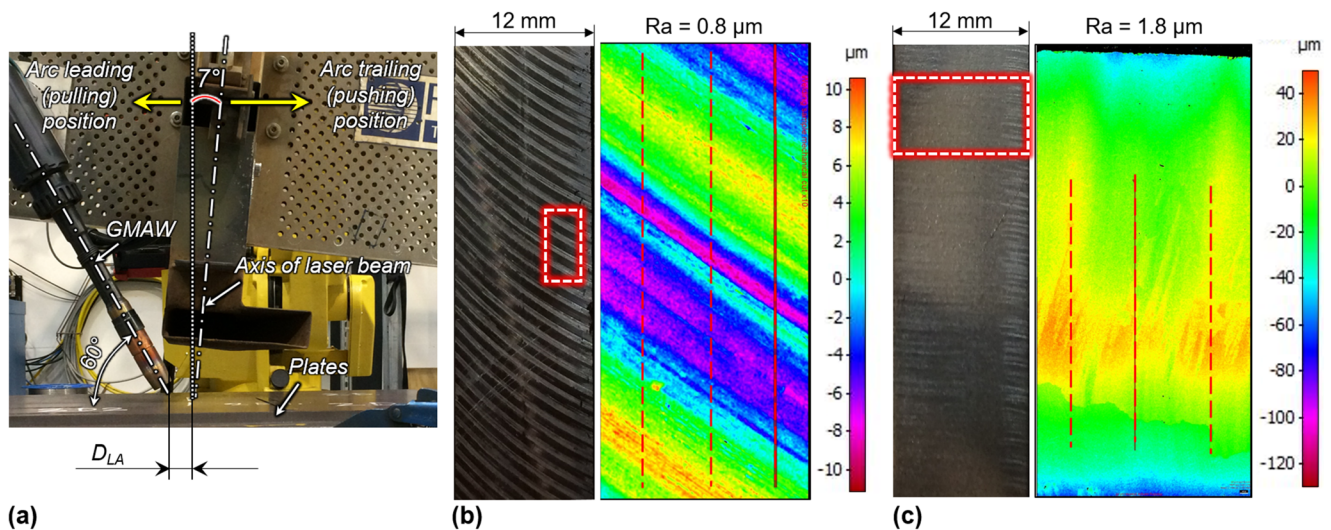


Fig. 1 a Experimental setup. Morphology and parameters of b machined and c plasma cut sidewalls

recent results, Frostevarg [10] presented that LAHW often provides humping due to unfavorable melt dynamics in the weld pool and larger root width. However, there is still many unknown factors why and how to avoid this very frequent problem in welding of thick plates. Application of electromagnetic backing can be as a solution [11–16]; however, its viability on a full industrial scale (for welds longer than 5–10 m) is of concern.

Narrow and deep welds tend to produce high hardness due to the fast cooling rates associated with low heat input. Partly, this is due to very small focused spot diameter which is typically 300–600 μm in diameter [17] with relatively high welding speeds. In welding of 20–25-mm carbon steel with 0.10 wt.% C, very high hardness (495 HV) was reported in both the weld metal (WM) and the coarse-grained heat affected zone (CGHAZ) [2]. Bunaziv et al. [4] reported hardness up to 360 HV in partial penetration welding of 45-mm thick steel in the root zone due to very fast cooling rates. Application of LAHW with an additional heat from the arc source can successfully reduce the hardness, e.g., < 280 HV in welding of 10-mm S420 MC grade steel (0.10 wt.% C) [18]. The weld metal hardness can be controlled by the welding wire through adjusting chemical composition, which should ideally produce the highest possible amount of acicular ferrite. Another option is to use preheating prior to welding. Turichin et al. [5] showed that preheating at 180 $^{\circ}\text{C}$ in root welding of 23.7-mm thick X80 grade steel (0.052 wt.% C) reduced the hardness

from 400 to 300 HV. As a result, high toughness level (> 50 J at -20°C) of the welds was achieved.

In the present work, a 16 kW disk laser was used to weld 12- and 15-mm thick plates with single-pass welding with the objective to study the effect of process parameters on the root formation and wire distribution in LAHW. So far, 15-mm thick plate welding has been very rarely studied, and the paper explicates some of the welding challenges and offer solutions for quality improvement. Microstructure characterization and mechanical testing were conducted and showed high mechanical properties of welds in a wide range of heat inputs. Based on a general analysis, the application of both LBW and LAHW has a high potential in joining of > 10-mm thick plates which can significantly increase the cost-effectiveness of manufacturing.

2 Methodology

2.1 Welding equipment and setup

A continuous wave randomly polarized 16-kW multi-mode disk laser (TruDisk16002 TRUMPF) was used in the experiments with the following parameters: fiber core diameter 200 μm , beam parameter product 8-mm·mrad, and 1030-nm wavelength. The laser beam had 600-mm focal length, focused to a spot size of 300 μm in diameter (as measured). The laser beam longitudinal inclination angle was 7° from normal towards the welding surface to eliminate back reflections. A gas metal arc welding (GMAW) torch was tilted by max. of 60° to the welding surface to eliminate impingement with a laser beam at closer distances. The welds were deposited with an articulated robot. The LAHW setup is shown in Fig. 1a, with geometrical setup parameters listed in Table 1.

Table 1 Constant geometrical and process welding parameters

| Parameter | Value and dimension |
|--------------------------------------|----------------------------|
| Filler wire stick-out | 20 \pm 1 mm |
| Laser-arc interdistance (D_{LA}) | 15 mm |
| Shielding gas composition | 80% Ar + 20% CO_2 |
| Shielding gas flow rate | 25 l/min |

Table 2 Chemical composition (wt.%) according to mill certificate values

| Material | C | Si | Mn | P | S | Ni | Nb | V | Ti | Fe |
|-------------|------|------|------|-------|-------|------|------|------|------|------|
| Base metal* | 0.14 | 0.50 | 1.60 | 0.020 | 0.015 | – | 0.05 | 0.10 | 0.05 | Bal. |
| Wire | 0.06 | 0.35 | 1.41 | 0.011 | 0.017 | 1.48 | – | – | – | Bal. |

*Maximum values and the steel also contains up to 0.02 wt% Al

2.2 Materials

The steel plates were received in 12- and 15-mm thicknesses with the same chemical composition. These were cut to dimensions 500 mm × 150 mm prior to preparation for welding. The base metal is thermomechanically rolled structural steel with a banded ferrite-pearlite microstructure which is suitable for low temperature applications with toughness of 40 J at –60 °C. Two different bevelling procedures were used, namely machined and plasma cutting, the latter as a much cheaper option. The morphology of the sidewalls is shown in Fig. 1b, c. The parameters of the surfaces for machined/plasma cut sidewalls, based on three measurement lines for each case, are as follows: average roughness of profile 0.8/1.8 μm (R_a), average height of profile (includes waviness of the surface) 4.0 μm/10.0 μm (P_a), and mean peak to valley height of primary profile 15 μm/24 μm (P_z). The effect of surface roughness of weld quality was rarely studied. According to Sokolov et al. [19], the particular range of surface roughness can significantly enhance penetration depth. However, the root quality was not elucidated. The sidewalls were cleaned with acetone to remove grease prior to welding. Tack welds were used to attach run-in and run-out plates. A commercial 1.2-mm metal-cored wire was selected, designed for low temperature applications (min. 47 J at –60 °C). The steel and filler wire chemical compositions and mechanical properties are shown in Table 2 and Table 3 respectively. The base metal has a carbon equivalent value of 0.25 ($P_{cm} < 0.14$ wt.% C, $P_{cm} = C + Si/30 + (Mn + Cu + Cr)/20 + Ni/60 + Mo/15 + V/10 + 5B$) and max. 0.38 (CE_{IIW} for low alloy steels, $CE_{IIW} = C + Mn/6 + (Cr + Mo + V)/5 + (Cu + Ni)/15$) representing good weldability.

2.3 Process variables

The total line energy input for LAHW (denoted as Q_H) is calculated as a sum of the laser beam (Q_L) and the arc energy input (Q_A) see Eq. 1. The arc efficiency factor (η_A) is 0.8 for

the GMAW process, while laser beam absorption coefficient (η_L) is 0.7 (due to reflections, heat conduction losses, laser power attenuation and scattering (Rayleigh and Mie scattering) by weld plume [20–23], and laser beam partly going through the keyhole exit [24]).

$$Q_H = Q_L + Q_A = \frac{60 \cdot P_L \cdot \eta_L}{1000 \cdot v_t} + \frac{60 \cdot P_A \cdot \eta_A}{1000 \cdot v_t} \quad (1)$$

where P_L is laser power (in kW), P_A is arc power (in kW: current multiplied by voltage), and v_t is travel speed (mm/min).

The experiment was conducted to achieve imperfection-free welding with maximum possible productivity (high welding speed) for reaching maximum potential of the process. A systematic variation, the one-variable-at-time (OVAT) method is not viable for LAHW due to many process parameters involved and limited testing program. The parameters include two different thicknesses and two welding processes (LBW and LAHW). Therefore, the parameter variation is based on one or two main parameters and one or two minor parameters adjustments, representing the serial design of experiments comparable experimental runs. In special cases, three main adjustments were involved to elucidate wider parameter ranges. Main parameter adjustment was the welding speed, the laser beam power, and/or the air gap. The minor parameter adjustment is related only with slight increase of arc power or wire feed rate (WFR) which has a marginal effect on process stability and overall quality of welds. The variable parameters are presented in Tables 4 and 5 for 12- and 15-mm thick plates respectively. As the main variable, the heat input was selected which is a function of welding speed (meaning travel speed of heat source/–s) and power level of the heat sources. In addition, it strongly influences the microstructure formation and process stability. Therefore, experiments were performed based on sequential change of total heat input (increase/decrease in Q_H) except the cases where arc is added/removed from process for direct comparison.

Table 3 Mechanical properties according to mill certificate values

| Material | Yield strength $R_{p0.2}$, MPa | Ultimate tensile strength R_m , MPa | Break elongation A_5 , % |
|------------|---------------------------------|---------------------------------------|----------------------------|
| Base metal | 420 | 520–680 | 19 |
| Wire | 518 (min. 460) | 598 (min. 530) | 31 (min. 20) |

Different arc positions and arc modes are also tested since they can affect the weld quality [25, 26].

The synergy lines of the used three different arc modes are illustrated in Fig. 2 (based on welding data after process), representing linear increase of current and voltage with increasing wire feed rate regardless of the arc mode.

2.4 Testing and characterization

Destructive testing was performed on a few welds including bending, tensile, and impact toughness. Bend testing was performed according to EN ISO 5173 [27] based on transverse side bending of butt joint (SBB) subjected to 180° angle bend, with standard specimen geometry and dimensions (12/15 × 10 × 300 mm³), bending die radius diameter was 25 mm. Cross weld tensile testing was performed based on EN ISO 4136 [28] using the standard specimen geometry and dimensions (shown in Fig. 3a). Prior to bending and tensile testing, the root humping was removed by milling, while the upper part only excessive reinforcement was removed. This means that eventual underfill and undercuts were included during testing.

The Charpy V-notch (CVN) impact toughness testing was performed according to ISO 9016 [29] with standard specimen dimensions of 55 × 10 × 10 mm³ and the standard V-notch type geometry. Two test series were included; one with the notch located in the WM center, and one positioned at the fusion line (FL). The Charpy samples were cut from the lower part of the weld which typically consists of the laser part, with their length axis in the transverse direction in the plate. The notch was placed perpendicular to the welding direction, providing a fracture path along the welding. All tests were performed at −50 °C, using three parallels for each experiment. The locations of extracted specimens are shown in Fig. 3b, c for WM and FL, respectively. The placement of the V-notch is challenging for FL, and etching was therefore performed before machining and placement of the notch.

Metallographic samples were prepared and examined according to the ISO 17639 [30] standard, involving cutting of weld macros (cross sections), grinding, polishing, and etching in 2% Nital. These were subsequently examined with optical microscope. Vickers microhardness (HV_{0.5}) measurements were made with a 500-gf load according to the ISO 22826 [31] standard.

Table 4 Welding parameters used for 12-mm thick plates

| Welding method | Weld No. | Air gap (mm) | Laser power (kW) | FPP (mm) | Welding speed (m/min) | Arc mode | WFR (m/min) | Arc position | Line energy input (kJ/mm) | | | |
|-------------------------------|----------|--------------|------------------|----------|-----------------------|----------|-------------|--------------|---------------------------|-------|-------|--|
| | | | | | | | | | Q_L | Q_A | Q_H | |
| Plasma cut edges (<i>P</i>) | | | | | | | | | | | | |
| LBW | 1P | 0.0 | 12 | 0 | 1.5 | – | – | – | 0.34 | – | 0.34 | |
| LAHW | 1AP | 0.0 | 12 | 0 | 1.5 | P | 14 | T | 0.34 | 0.39 | 0.73 | |
| LAHW | 2P | 0.0 | 12 | 0 | 2.0 | P | 14 | L | 0.25 | 0.29 | 0.55 | |
| LAHW | 3P | 0.5 | 16 | 0 | 2.0 | S | 16 | L | 0.34 | 0.41 | 0.75 | |
| LAHW | 4P | 0.5 | 16 | 0 | 1.8 | S | 12 | L | 0.37 | 0.39 | 0.77 | |
| LAHW | 5P | 0.0 | 16 | 0 | 1.6 | S | 12 | L | 0.42 | 0.44 | 0.86 | |
| Arc | 5P | 0.0 | – | – | 0.5 | C | 6 | Pulling | – | 0.29 | 0.29 | |
| LBW | 5AP | 0.0 | 16 | 0 | 1.6 | – | – | – | 0.42 | – | 0.42 | |
| Arc | 5AP | 0.0 | – | – | 0.5 | C | 6 | Pulling | – | 0.29 | 0.29 | |
| Machined edges (<i>M</i>) | | | | | | | | | | | | |
| LAHW | 1M | 0.0 | 16 | 0 | 1.6 | C | 6 | L | 0.42 | 0.10 | 0.52 | |
| Arc | 1M | 0.0 | – | – | 0.5 | S | 5 | Pulling | – | 0.31 | 0.31 | |
| LBW | 2M | 0.0 | 16 | 0 | 1.6 | – | – | – | 0.42 | – | 0.42 | |
| Arc | 2M | 0.0 | – | – | 0.5 | S | 5 | Pulling | – | 0.31 | 0.31 | |
| LAHW | 3M | 0.5 | 14 | 0 | 1.5 | C | 8.33 | L | 0.39 | 0.16 | 0.55 | |
| LAHW | 4M | 0.5 | 12 | 0 | 1.5 | C | 8.33 | L | 0.34 | 0.16 | 0.50 | |
| LAHW | 5M | 0.0 | 10 | 0 | 1.0 | S | 2 | L | 0.42 | 0.06 | 0.48 | |
| Arc | 5M | 0.0 | – | – | 0.5 | S | 8 | Pulling | – | 0.59 | 0.59 | |
| LAHW | 6M | 0.0 | 16 | +25 | 0.9 | S | 2 | L | 0.75 | 0.07 | 0.82 | |
| Arc | 6M | 0.0 | – | – | 0.5 | S | 9 | Pulling | – | 0.78 | 0.78 | |

P plasma cut, *M* machined, *P* pulsed, *S* standard, *C* CMT arc mode, *T* trailing arc, *L* leading arc. *FPP* is focal point position (plus sign indicates defocused laser)

Table 5 Welding parameters used for 15-mm thick plates

| Welding method | Weld No. | Air gap (mm) | Laser power (kW) | FPP (mm) | Welding speed (m/min) | Arc mode | WFR (m/min) | Arc position | Line energy input (kJ/mm) | | |
|-------------------------------|----------|--------------|------------------|----------|-----------------------|----------|-------------|--------------|---------------------------|----------------|----------------|
| | | | | | | | | | Q _L | Q _A | Q _H |
| Plasma cut edges (<i>P</i>) | | | | | | | | | | | |
| LBW | 1PF | 0.0 | 12 | 0 | 1.0 | – | – | – | 0.50 | – | 0.50 |
| LAHW | 2PF | 0.0 | 12 | 0 | 1.1 | C | 6 | L | 0.46 | 0.13 | 0.59 |
| LAHW | 3PF | 0.5–1.0 | 12 | 0 | 2.0 | S | 14 | L | 0.25 | 0.38 | 0.64 |
| LAHW | 4PF | 0.5–1.0 | 13 | 0 | 2.0 | S | 15 | L | 0.27 | 0.38 | 0.66 |
| LAHW | 5PF | 0.5 | 14 | 0 | 2.0 | S | 14 | L | 0.29 | 0.38 | 0.68 |
| LAHW | 6PF | 0.5 | 14 | 0 | 1.5 | S | 14 | L | 0.39 | 0.51 | 0.90 |
| LAHW | 7PF | 0.0 | 16 | 0 | 1.5 | S | 12 | L | 0.45 | 0.47 | 0.92 |
| Machined edges (<i>M</i>) | | | | | | | | | | | |
| LAHW | 1MF | 0.0 | 16 | 0 | 1.5 | S | 12 | L | 0.45 | 0.47 | 0.92 |
| LAHW | 2MF | 0.0 | 16 | 0 | 1.8 | S | 14 | L | 0.37 | 0.43 | 0.80 |
| LAHW | 3MF | 0.5 | 16 | 0 | 2.0 | S | 14 | L | 0.34 | 0.38 | 0.72 |
| LAHW | 3AMF | 0.5 | 16 | 0 | 2.0 | S | 14 | T | 0.34 | 0.38 | 0.72 |
| LAHW | 3BMF | 0.5 | 14 | 0 | 2.0 | S | 14 | L | 0.29 | 0.38 | 0.68 |
| LAHW | 3CMF | 0.5 | 16 | 0 | 2.0 | S | 14 | L | 0.34 | 0.38 | 0.72 |
| LAHW | 3DMF | 0.5 | 16 | 0 | 2.0 | S | 16 | L | 0.34 | 0.41 | 0.75 |
| LAHW | 3EMF | 0.5 | 16 | 0 | 1.8 | S | 14 | L | 0.37 | 0.43 | 0.80 |
| LAHW | 4MF | 0.5 | 16 | 0 | 2.2 | S | 16 | L | 0.31 | 0.37 | 0.68 |
| LAHW | 5MF | 1.0 | 12 | 0 | 2.0 | P | 16 | L | 0.25 | 0.35 | 0.60 |
| LAHW | 6MF | 1.0 | 12 | 0 | 2.0 | P | 20 | L | 0.25 | 0.38 | 0.63 |
| LAHW | 7MF | 1.5 | 12 | 0 | 2.5 | P | 18 | L | 0.20 | 0.29 | 0.49 |
| LAHW | 8MF | 1.5 | 12 | +25 | 2.5 | P | 18 | L | 0.20 | 0.29 | 0.49 |

P plasma cut, *M* machined, *P* pulsed, *S* standard, *C* CMT arc mode, *T* trailing arc, *L* leading arc. *FPP* is focal point position (plus sign indicates defocused laser)

3 Results and discussion

3.1 Welding of 12-mm thick plates

3.1.1 Process stability and weld quality

The weld macrographs for the 12-mm thick plate are shown in Fig. 4 for the plasma cut sidewalls with sequentially adjusted process parameters. The autogenous LBW (without filler wire) was applied with full penetration and good quality of

welds with high quality consistency through a whole weld length (Weld No. 1P). This weld is qualified to level B according to ISO 13919–1 [32] standard. A slight undercut was found at the top surface due to gravity but is still within the range of acceptance (< 0.5 mm). Underfilling and undercuts are very common in LBW where filler wire is not used. Underfilling is mostly related to melt dropouts caused by gravity effect [9, 10]. The same parameters were applied with the arc added (LAHW, Weld No. 1AP) to the process. Severe root humping occurred with extended large laser-arc distance

Fig. 2 Synergy lines for different arc modes based on average **a** current and **b** voltage values

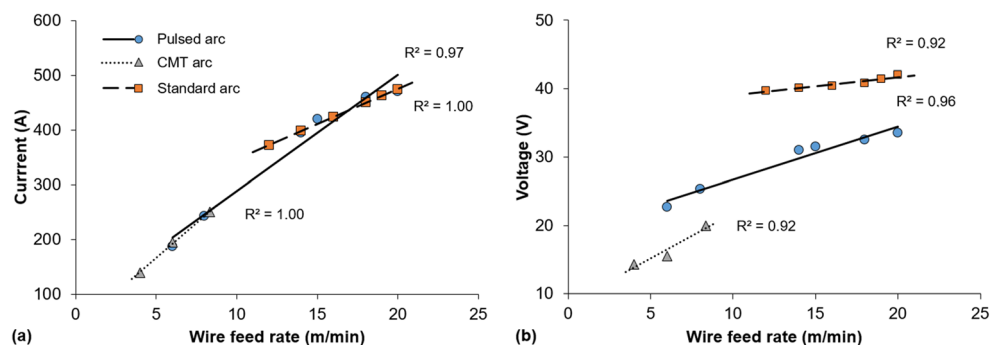
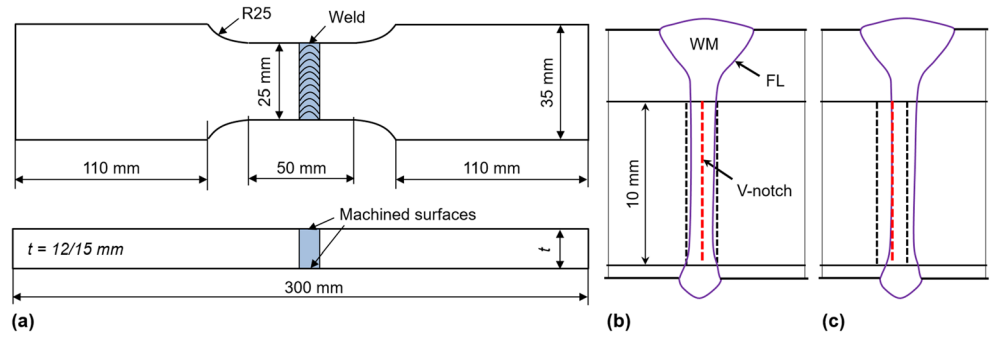


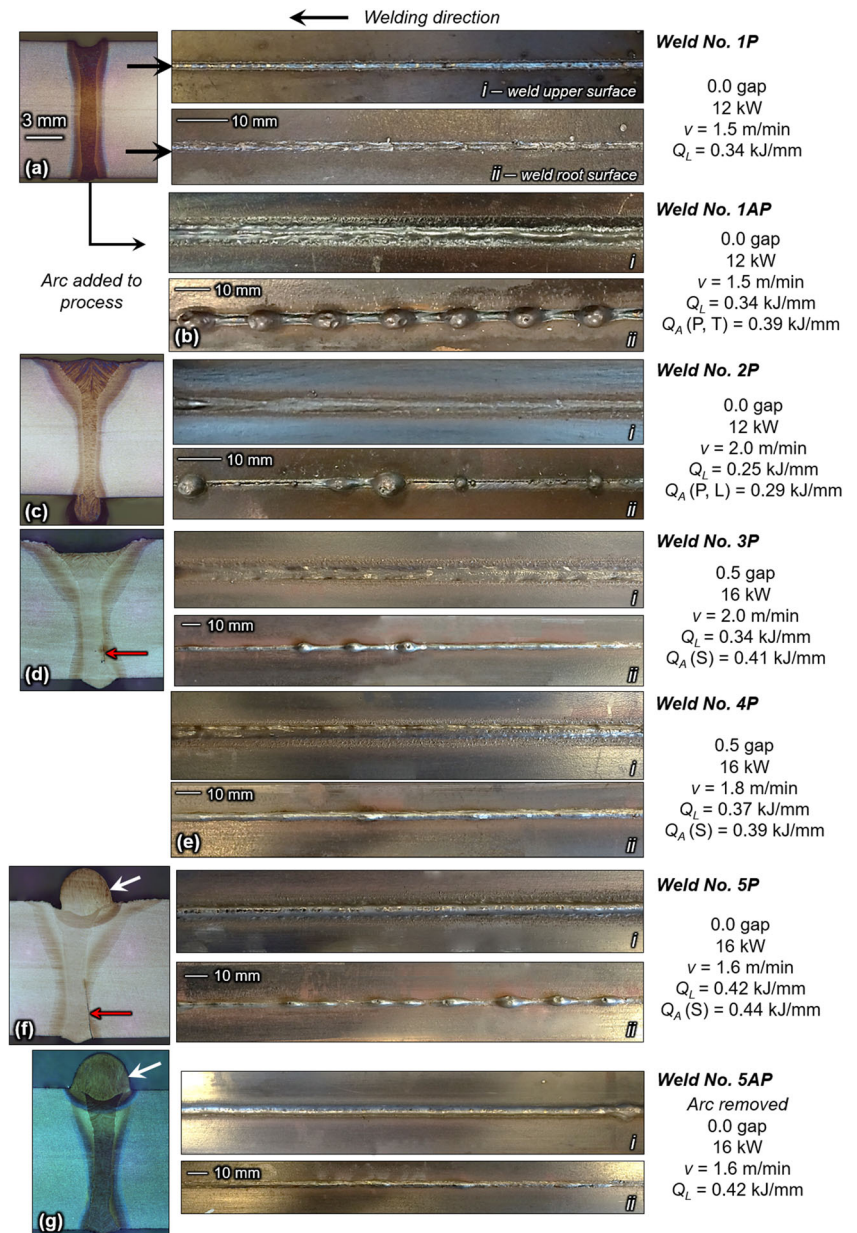
Fig. 3 a Dimensions of tensile specimen. Charpy V-notch location and specimen extraction for b weld metal and c fusion line



(15 mm), whereas the typical value is in the range of 2–6 mm [33]. According to ISO 12932 [34], the root humping is not acceptable within the following range for level B: hump

height = 1.0 mm + 0.3 × width of the root. To suppress humping, the welding speed was increased to 2.0 m/min, and the arc position was changed to leading (Weld No. 2P).

Fig. 4 Welding of 12-mm thick plate, weld cap, and weld root appearances with plasma cut sidewalls

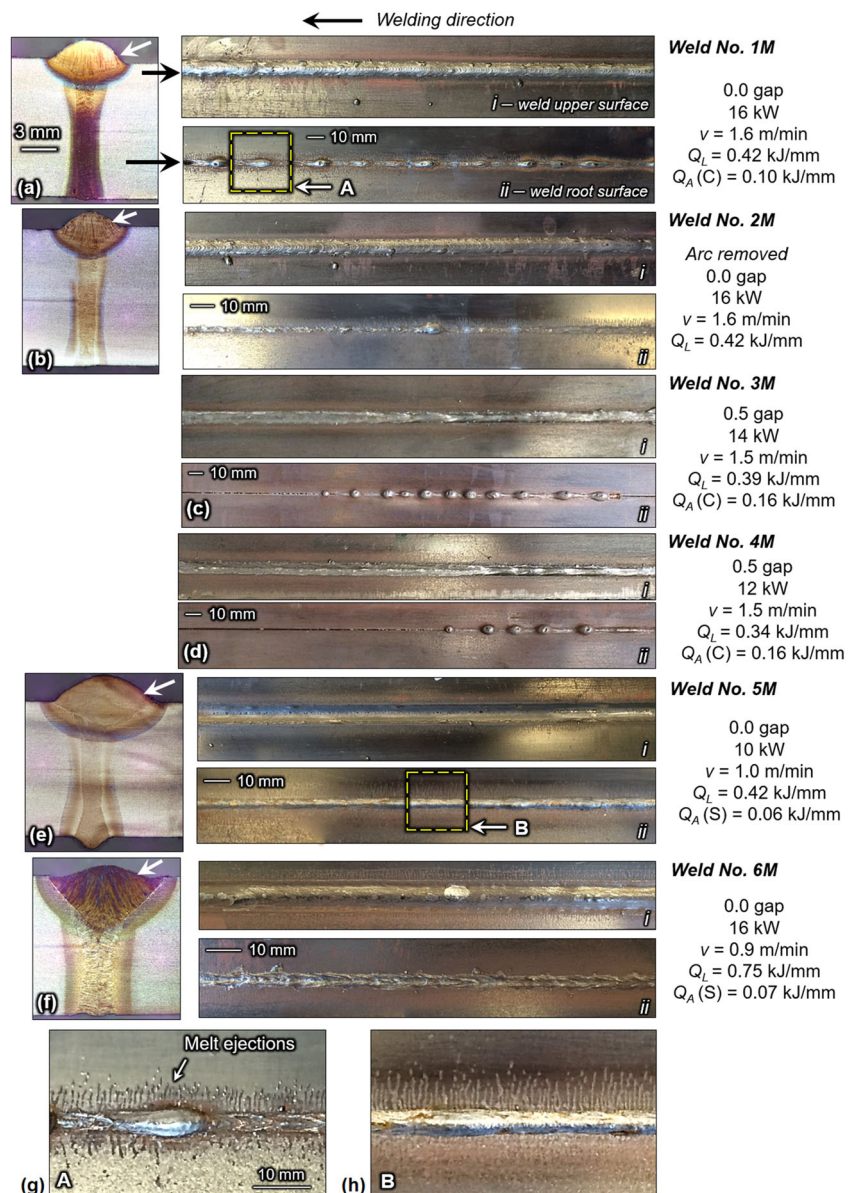


As a result, humping was slightly mitigated. However, it provided inconsistent penetration depth. This can be related to variations in plasma cut edge quality and low laser beam power used. After a subsequent adjustment of the laser power and travel speed, good root quality was achieved (Fig. 4e, g). Increasing the root width and air gap can cause higher tendency to root humping or sagging due to gravity. This has been shown in single-pass LAHW of both 12-mm steel [10]. However, in case of similar fusion zone width in the root area, humping has high probability to occur. Based on the work by Haug et al. [9], it was shown that melt flow dynamics can play a significant role, especially in application of 1030-nm wavelength laser beam source. The macrographs examined did not show any surface cracking or pores in any of the welds. One important disadvantage of the plasma cut preparation is a

frequent lack of fusion with sidewalls (indicated by red arrows in Fig. 4d, f) which may be related to uneven transversal geometry associated with small deviation of perpendicularity to the plate surface.

Macrographs of welds with machined sidewalls are shown in Fig. 5. Humping frequently occurred when fast travel speed (> 1.5 m/min) and high laser power (14–16 kW) were applied. Humping was reduced by application of a tandem welding technique, where the autogenous LBW was followed by the arc as a second pass. In this way, harmful effects of the arc source were mitigated (Weld. No 2 M). When the laser beam drills vapor cavity through the whole plate by achieving full penetration condition, the melt ejections are clearly visible as spattering (indicated by area A in Fig. 5a, see magnification of area in Fig. 5g). Moreover, the arc source also produced melt

Fig. 5 Welding of 12-mm thick plate, weld cap, and root surface appearances with machined sidewalls. Magnification of areas A and B is shown in (g) and (h), respectively



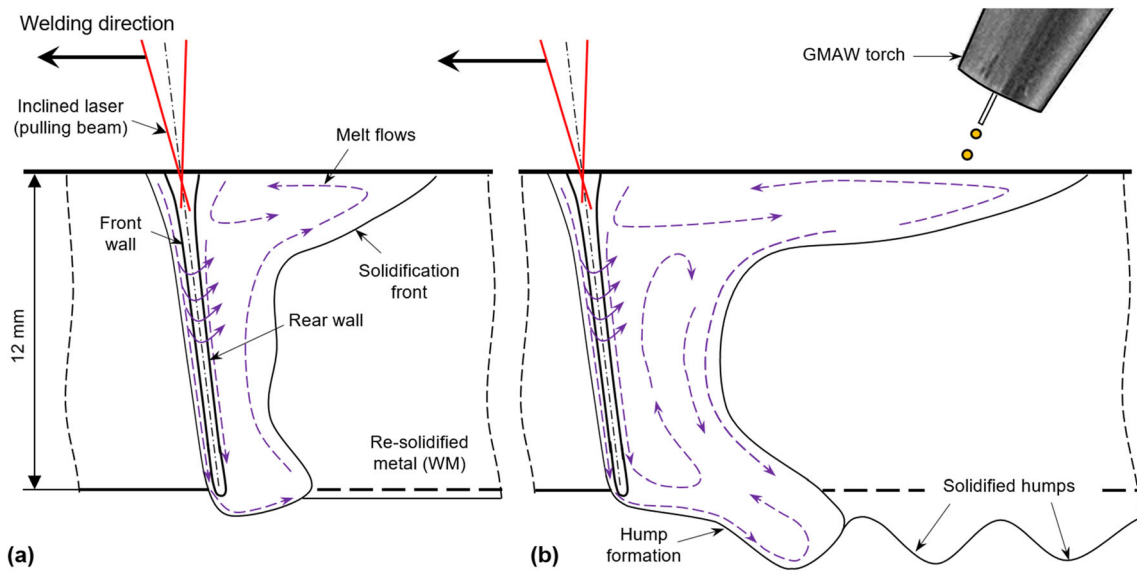


Fig. 6 Comparison of LBW and LAHW: **a** weld pool of LBW (Weld No. 1P); **b** weld pool humping in LAHW with trailing arc position setup (Weld No. 1AP)

ejection-like spattering (indicated by area *B* in Fig. 5e with magnification of area in Fig. 5h), indicating unstable arc condition related to fast welding speeds. Ejections in the root appeared more frequently in machined sidewall specimens. This shows that the sidewall quality affects the process conditions. Another way to eliminate root humping is to apply higher laser power combined with slower travel speed (< 1.2 m/min, see Fig. 5f). However, the process enters to constant melt ejection mode [9] and a higher portion of laser power goes through the plates resulting in lower effectiveness of the process. This fact is also reflected through the same size of HAZ even though the heat input was almost doubled. Moreover, undercut in the root can also be present in such welds.

An illustration of the proposed physical explanation of the humping phenomenon is shown in Fig. 6. The arc in the LAHW process affects the melt flow by increasing its

momentum (the mass momentum) towards the root. This can also be related to an enhanced arc pressure due to higher currents applied [35] even though a 15-mm laser-arc distance was used. The amount of molten metal in the weld pool determines mass momentum in combination with forces acting on it. As an example, in welding of thin plates, mass momentum is much lower, thus the toroid-shaped keyhole is created where the surface tension is dominating [36, 37].

Based on the performed experiments, the processing maps can be established for plasma cut and machined sidewalls Fig. 7 and Fig. 8 respectively. The processing regions are separated by dashed lines. The acceptable process window tends to be narrow, where good results were only achieved by balanced adjustment of parameters towards lower laser beam power combined with reduced welding speed. Welding with zero air gap showed better results since it may lower pressure in the keyhole, and laser beam is partially

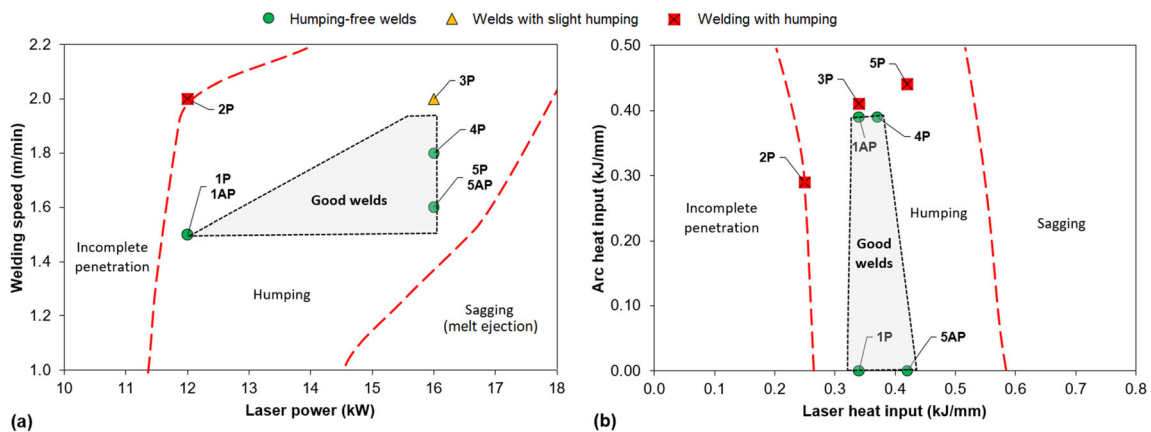


Fig. 7 Processing maps for 12-mm plate with plasma cut sidewalls: **a** effect of laser power and welding speed and **b** effect of laser-to-arc heat ratio. Indicated area shows acceptable processing window

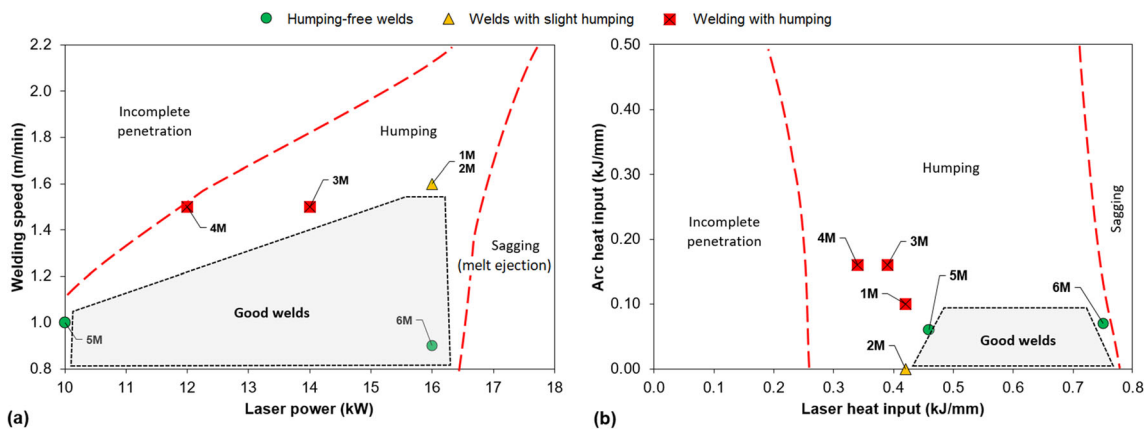


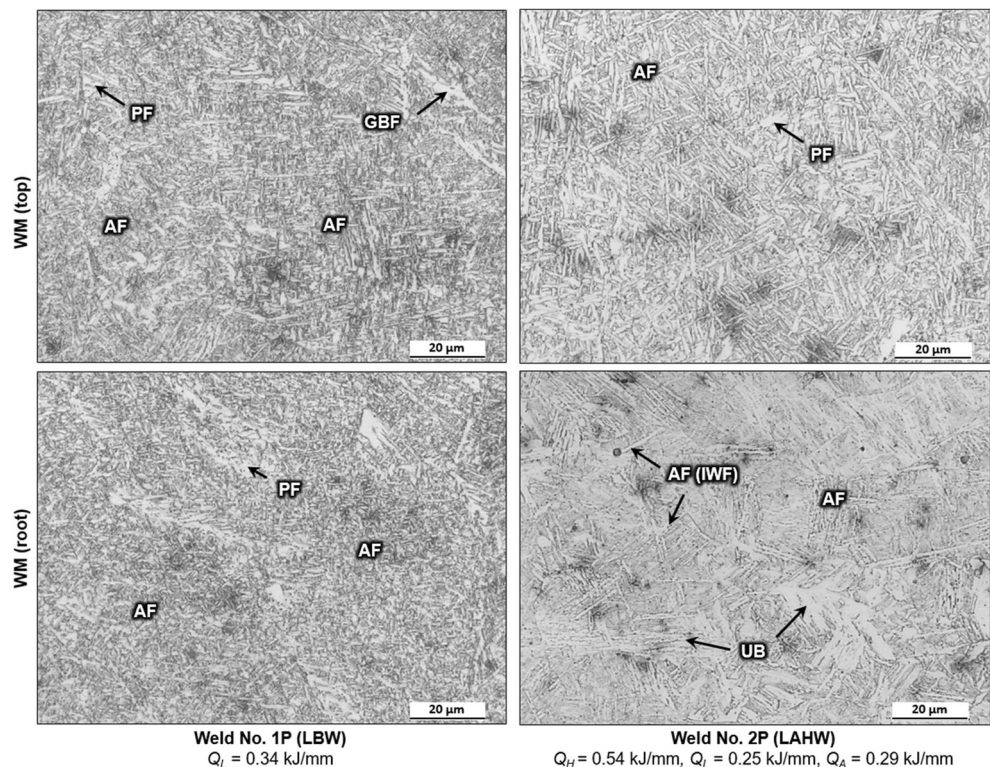
Fig. 8 Processing maps for 12-mm plate with machined sidewalls: **a** effect of laser power and welding speed and **b** effect of laser-to-arc heat ratio. Indicated area shows acceptable processing window

transmitted through the plates. Welding with an air gap is more complex and apparently not very reliable since it may be difficult to keep it constant during production. Moreover, use of an air gap showed inconsistent quality of the root with periodic humping, especially for plasma cut sidewalls. Leading arc position (when laser is trailing) showed better results compared with trailing arc setup (when laser is leading). Similar results were concluded by Tang et al. [38] by claiming that leading arc provided better melt dynamics corresponding to slower melt velocities in the root. Trailing arc position is not recommended with air gap due to lack of material for the keyhole to be created for the 15-mm laser-arc distance employed.

3.1.2 Microstructure and hardness

The microstructure of weld metals deposited with LBW had high-volume fraction of fine-grained acicular ferrite (AF) with some grain boundary ferrite (GBF) and polygonal ferrite (PF), see Fig. 9. The LAHW process provided similar microstructure. However, a slightly higher amount of GBF and PF was produced due to an increased cooling time ($\Delta t_{8/5}$, the range from 800 down to 500 °C) due to higher heat input. Moreover, the AF formed has more elongated ferritic platelets, which is more similar to intragranular Widmanstätten ferrite (IWF) than the typical interlocking fine-grained AF [39–41]. The high AF volume fraction in LBW is possibly caused by the

Fig. 9 Microstructure evolution in WM of lowest (0.34 kJ/mm) and highest heat input (0.54 kJ/mm) experiments in case of 12-mm thick plates. AF—acicular ferrite, PF—polygonal ferrite, UB—upper bainite



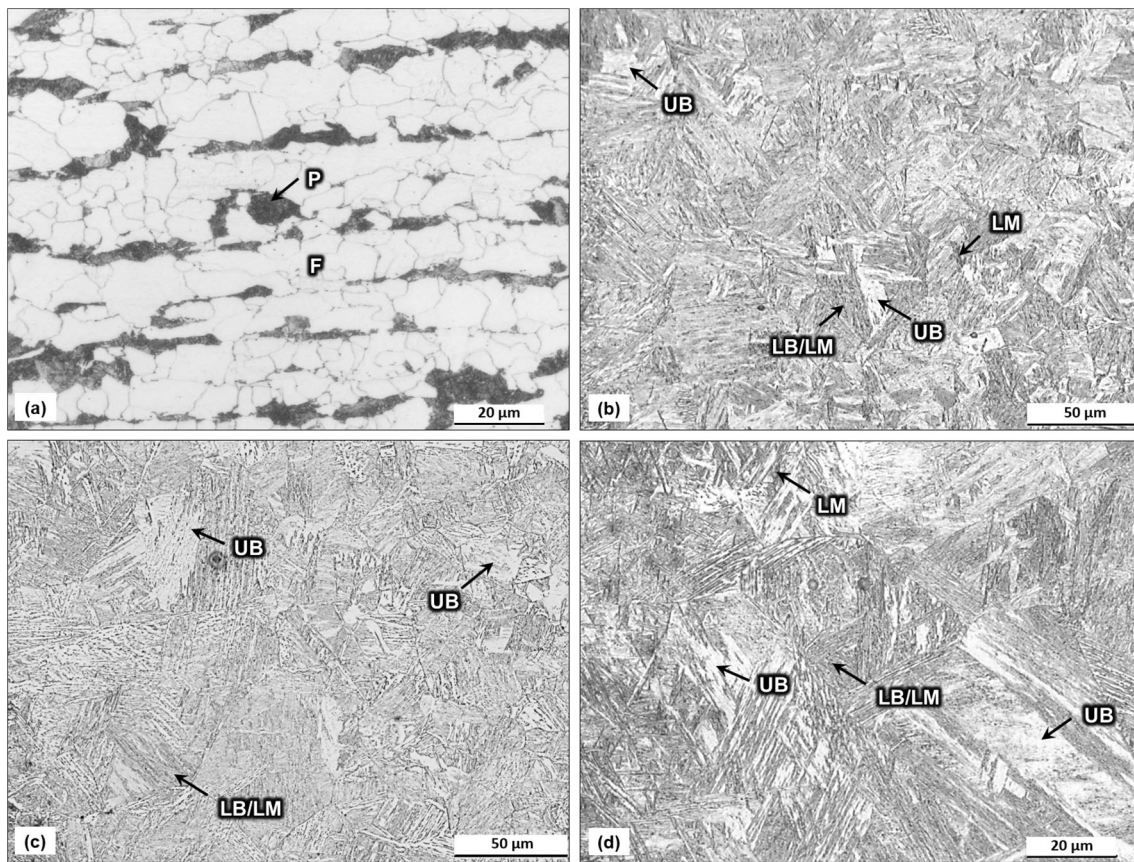


Fig. 10 Microstructure evolution in **a** BM, **b** CGHAZ of Weld No. 1P (root area), **c** CGHAZ of Weld No. 2P, and **d** CGHAZ of Weld No. 1P with high magnification. F—ferrite, P—pearlite, AF—acicular ferrite, PF—polygonal ferrite, UB—upper bainite, LB—lower bainite, LM—lath martensite

slightly faster cooling rate suppressing GBF and PF formation [42]. It is reasonable to assume that the AF formation takes

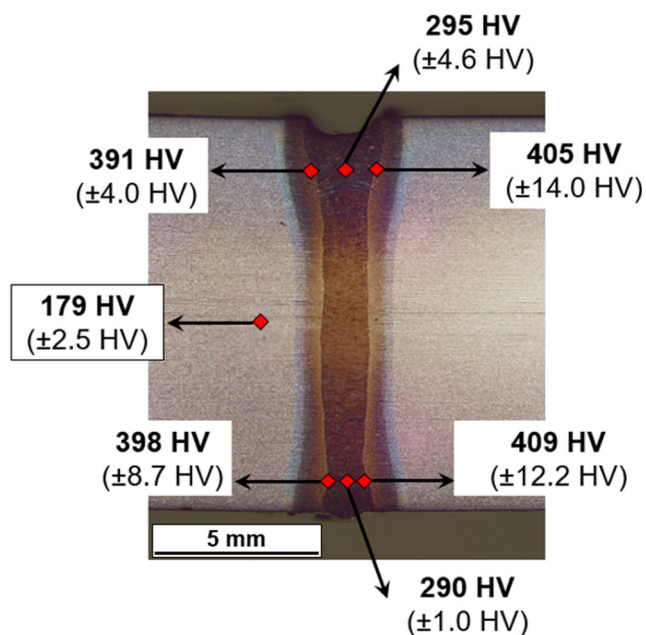


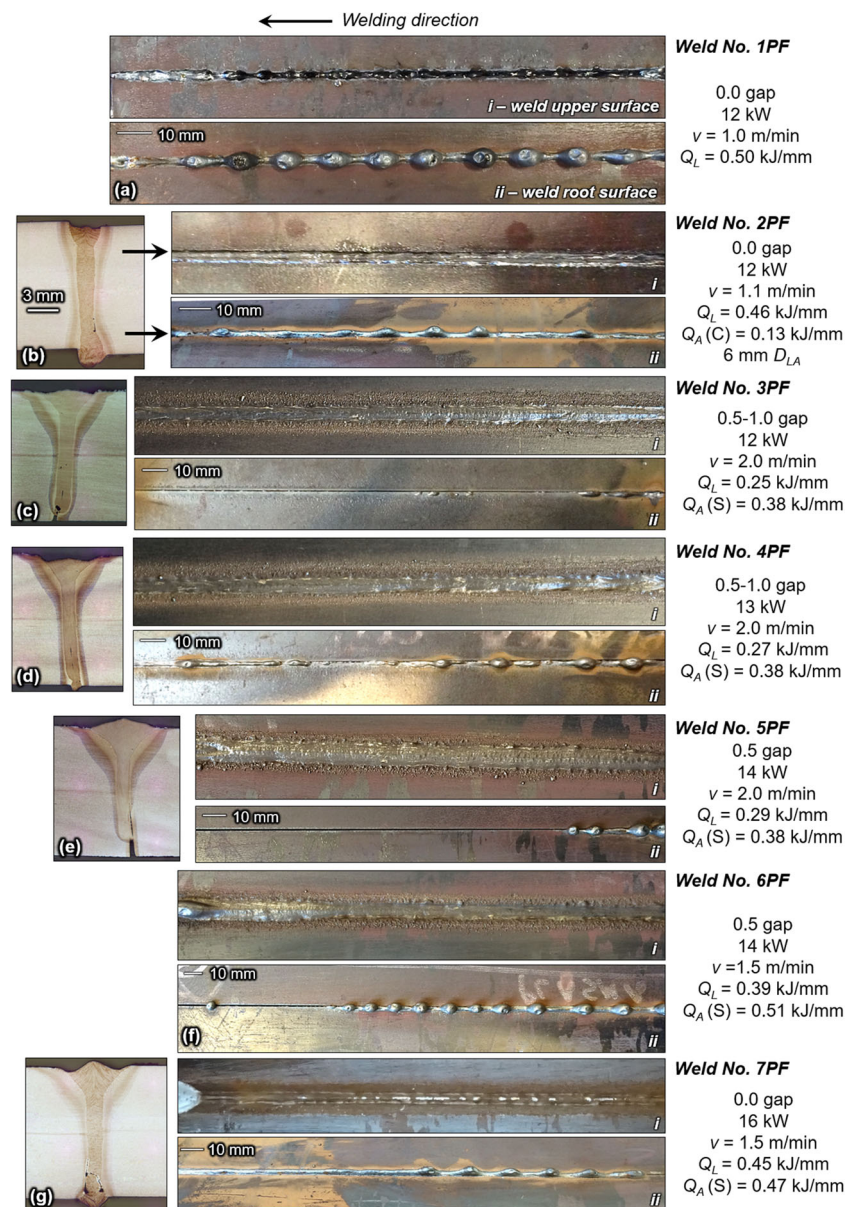
Fig. 11 Hardness of LBW joint (Weld No. 1P)

preferably place within a certain range of cooling time. For fast cooling time ($\Delta t_{8/5} < 3.0$ s), harder microstructures like bainite (UB/LB—upper/lower bainite) and lath martensite (LM) may be formed in the WM.

The BM microstructure shown in Fig. 10a consisting of typical banded ferrite-pearlite. In the CGHAZ micrograph (see Fig. 10b, c), the microconstituents are mainly upper bainite and lath martensite regardless of heat input. Lath martensite is visible in Fig. 10d (as darker areas) with higher magnification. However, lower heat input parameters (< 0.4 kJ/mm) provided smaller prior austenite grain size than those of high heat input parameters (> 0.5 kJ/mm).

The hardness results for ALBW welds are provided in Fig. 11. Substantial difference in hardness is achieved between WM and HAZ near FL. WM had low hardness up to 300 HV due to the AF formation, whereas up to 410 HV was measured in HAZ near FL. The latter value is very high and is not acceptable in welding procedure qualification. Application of preheating and post-weld heat treatment [5] is a potential solution but can be expensive. Moreover, it will cause larger HAZ width [43, 44]. Alternative solution is to use higher heat input from either the laser beam [16] or the arc power. However, this may lead to excessive penetration and

Fig. 12 Welding of 15-mm thick plate showing weld upper surface and weld root surface appearances with plasma cut sidewalls



spattering on the root side with underfill on the top [9]. A further decrease of the carbon content in the base metal (reduction of carbon equivalent CE) can effectively mitigate hardness. The measured hardness values are consistent with the microstructure observations.

3.2 Welding of 15-mm thick plates

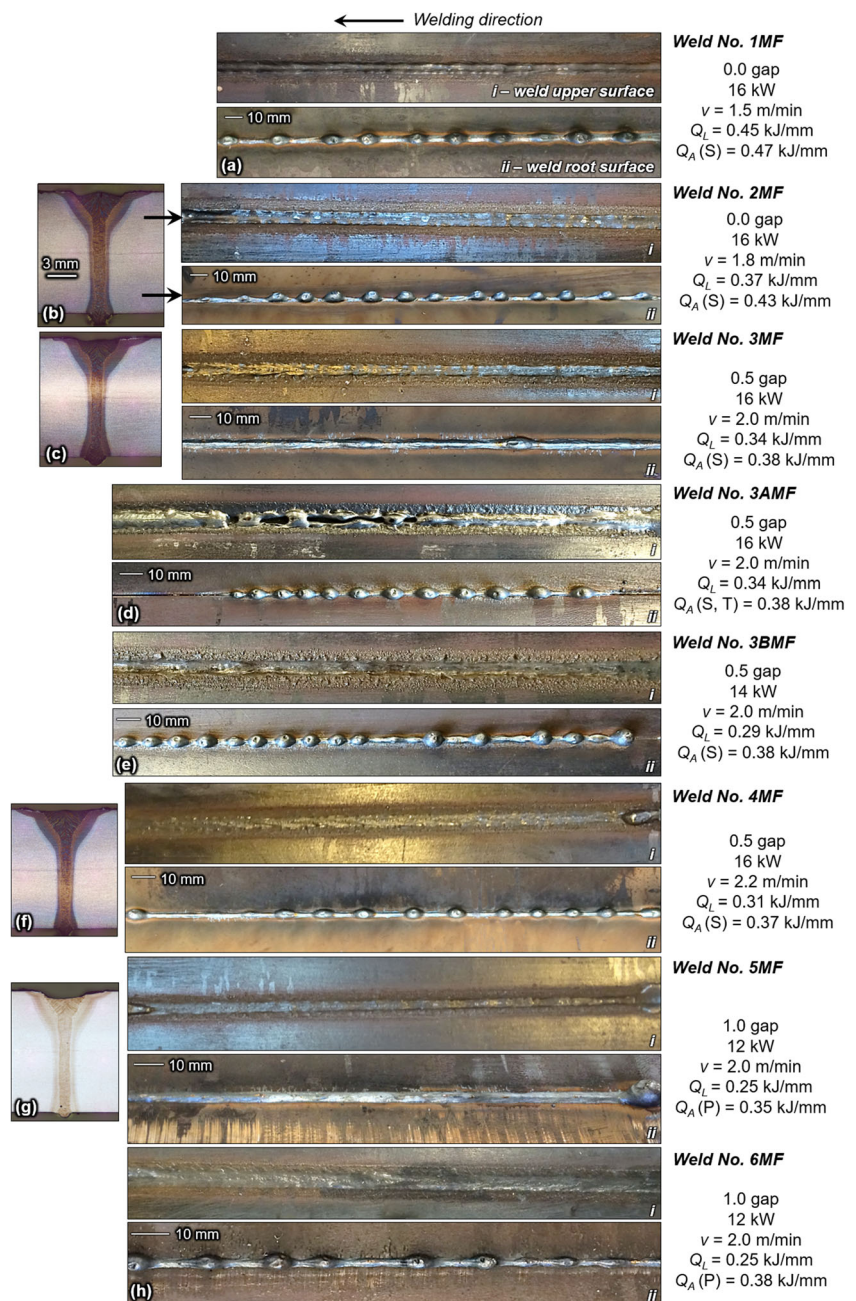
3.2.1 Process stability and weld quality

Macrographs and weld appearances of the welds for 15 mm using plasma cut sidewalls are shown in Fig. 12. Weld No. 1PF (Fig. 12a) had severe humping with strong underfill. It can be noted that, at the start and the end of weld, no humping occurred which can be related to complex molten pool

formation. When the CMT arc was added to the process (Weld No. 2PF, Fig. 12b) with slightly increased welding speed from 1.0 to 1.1 m/min, some minor intermittent humping was produced with much less underfill and humping. By increasing the laser power (from 12 to 14 kW) and welding speed (from 1.5 to 2.0 m/min) with standard arc mode (doubled WFR to make larger reinforcement), incomplete penetration occurred (Fig. 12c–f) due to lack of sufficient beam intensity. Weld. 7PF (Fig. 11g) demonstrated promising results at 1.5 m/min welding speed. However, the first half of the weld had humping, while the remaining length had good root quality. This can be related to stabilization of the process and clearly demonstrates the process sensitivity.

Weld No. 7PF was deposited with machined sidewalls (Weld No. 1MF) and severe humping occurred, as evident

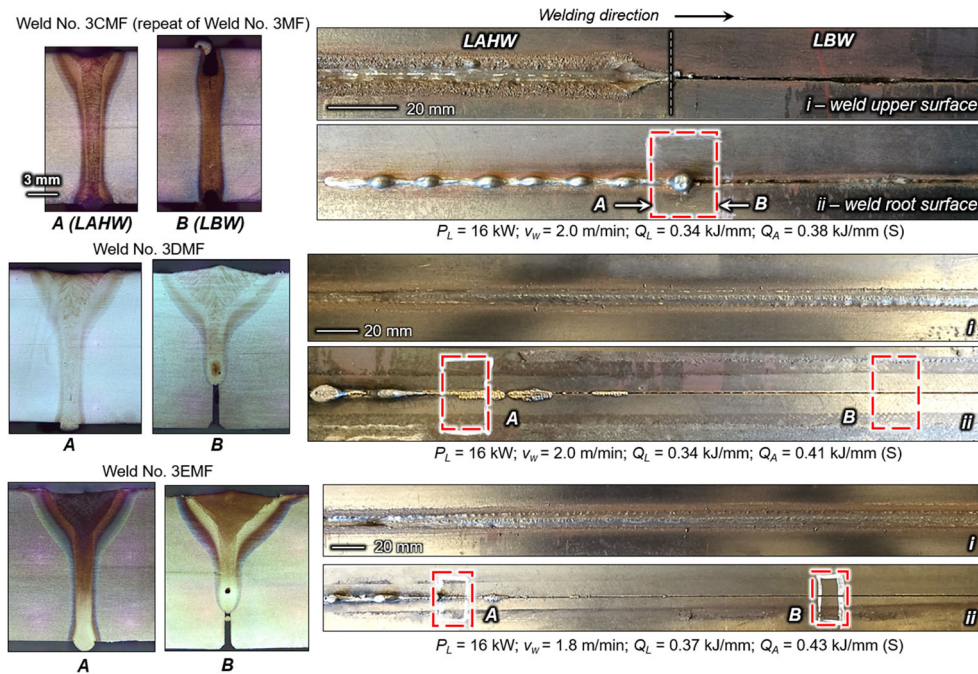
Fig. 13 Welding of 15-mm thick plate showing weld upper surface and weld root surface appearances with machined sidewalls



from the weld photo contained in Fig. 13a. This indicated that edge preparation can potentially affect the quality of the root, especially for thicker plates. However, the frequency of humps was slightly reduced as well as their height. In addition, the roughness of plasma cut sidewalls varied in the longitudinal direction which may explain the intermittence. With an increase of welding speed from 1.5 to 1.8 m/min (Weld No. 2MF, Fig. 13b) and a very slight increase of WFR, humping occurred more frequent. A further increase of welding speed to 2.0 m/min, combined with a 0.5 mm air gap (Weld No. 3MF, Fig. 13c), provided humping-free root. Despite the underfilling (too low WFR), welds can be qualified to a level

B according to the ISO 12932 [34]. Application of trailing arc (Weld No. 3AMF, Fig. 13d) provided humping and very unstable arc weld pool resulting in severe underfill. This observation may indicate that leading arc is preferable, especially with an air gap. A reduction of the laser beam power (to 14 kW) generated more humping (Weld No. 3BMF, Fig. 13e) since the process enters the dropping mode. Very similar trend was reported by Haug et al. [9]. Furthermore, by applying faster welding speed, intermittent humping occurred again (Weld No. 4MF, Fig. 13f), clearly indicating that an increase of welding speed is harmful to the process stability. The humping was successfully mitigated by increasing air gap

Fig. 14 Root appearance after removal of fiberglass backing



to 1.0 mm, changing in the arc mode to pulsed from standard, reducing welding speed from 2.2 to 2.0 m/min and laser power to 12 kW (Weld No. 5MF, Fig. 13g). Use of pulsed arc might be a better solution in combination of increase of air gap is positive together with a reduction of laser beam power and travel speed. However, an increased air gap requires adjustment of parameters in order to eliminate root dropouts and sagging. At this point, it is very difficult to understand if air gap is more positive in suppressing humping since controversial results are achieved. With application of air gap, there is possibly a lower pressure inside the keyhole root and the amount of molten metal providing more favorable melt flows redirecting extra molten material to the rear part of weld pool. This requires further investigation since there is very few papers published so far with very limited explanations [10, 45]. An increased air gap might reduce the pressure at the bottom

of the keyhole near the exit and improve melt flow dynamics, according to the high speed imaging studies from Ilar et al. [45]. A lower laser power might reduce the pressure near the keyhole exit resulting in more stable melt flow. When the WFR was raised to 20 m/min, intermitted humping was produced (Weld No. 6MF, Fig. 13h). It clearly shows that an increase in the WFR affects the melt flow conditions and promotes humping. In the last stage, with 1.5-mm gap (Weld No. 7–8MF), very poor weld quality was produced (severe underfill from both sides) due to narrow laser beam waist.

The optimized experiment (based on Weld No. 3MF) was repeated with application of fiberglass backing strip on the root side to stop root dropouts. The welds are shown in Fig. 14 and reveal poor stability and an extreme sensitivity of the process. The welds showed inconsistent quality based on penetration depth. At this point, the noticeable variation in

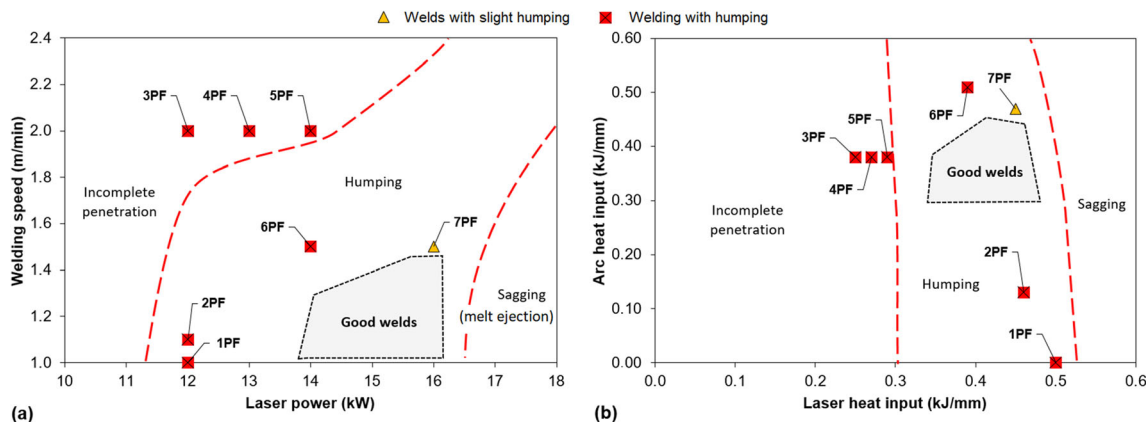


Fig. 15 Processing maps for 15-mm plate with plasma cut sidewalls: **a** effect of laser power and welding speed and **b** effect of laser-to-arc heat ratio. Indicated area shows potentially acceptable processing window

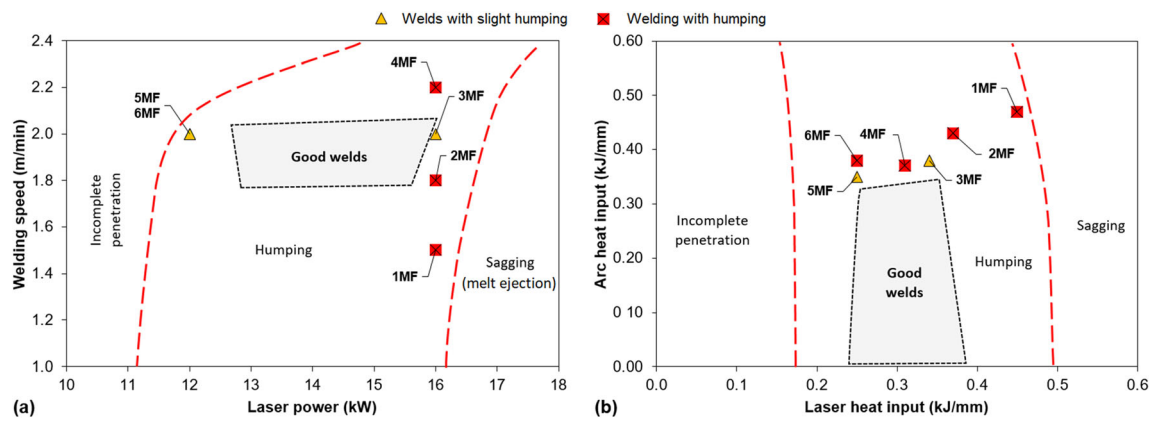


Fig. 16 Processing maps for 15-mm plate with machined sidewalls: **a** effect of laser power and welding speed and **b** effect of laser-to-arc heat input ratio. Indicated area shows acceptable processing window

penetration depth, even though air gap was consistent, cannot be explained clearly. It may be linked to accumulation of the filler wire (leading arc) around the keyhole resulting in increase of effective thickness and more laser power is required to achieve full penetration. The use of backing may allow wider air gap between the plates. However, the lack of bonding between the weld metal, and the

base metal on the backing side may lead to corrosion problems during service.

The processing maps (see Figs. 15 and 16) can be established based on experimental observations. To achieve good root quality, the main variables to consider are the laser power and the welding speed as well as balance of the laser heat input and the arc energy. The process window is narrow

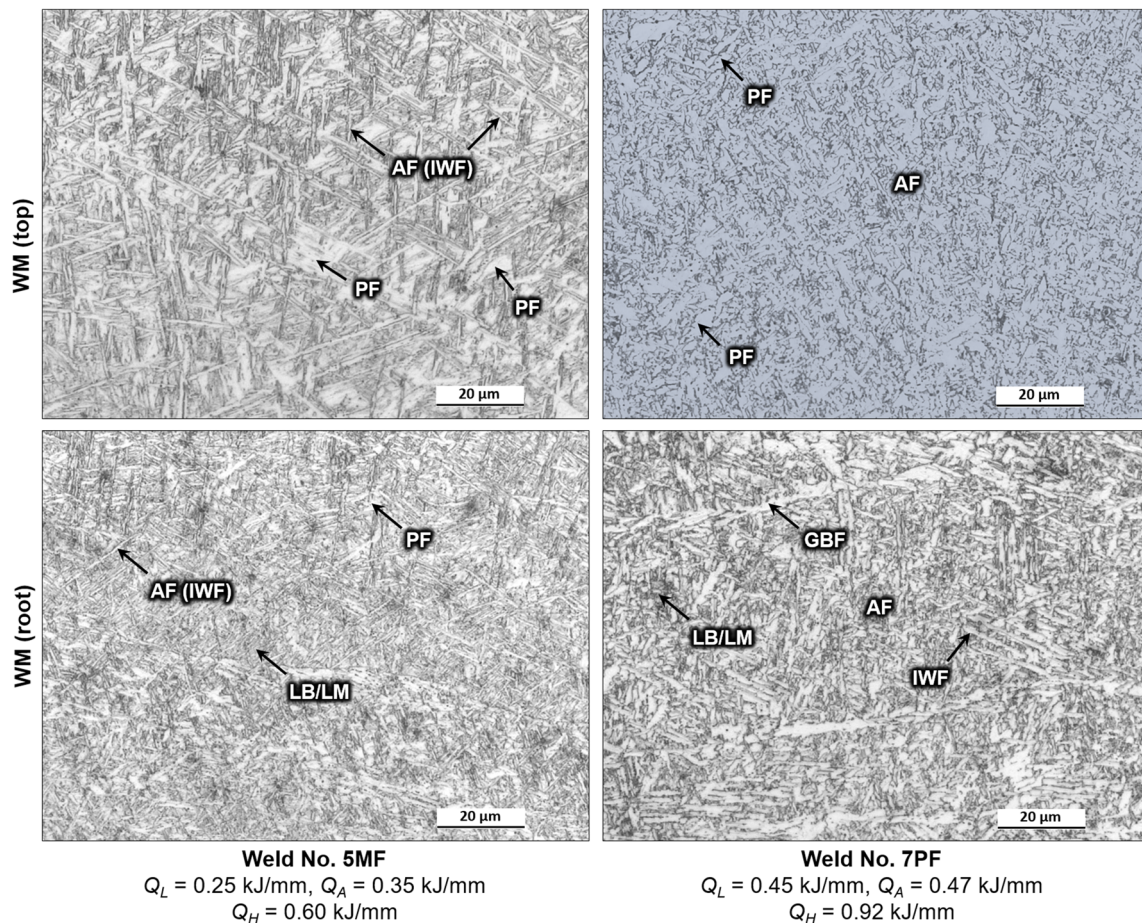
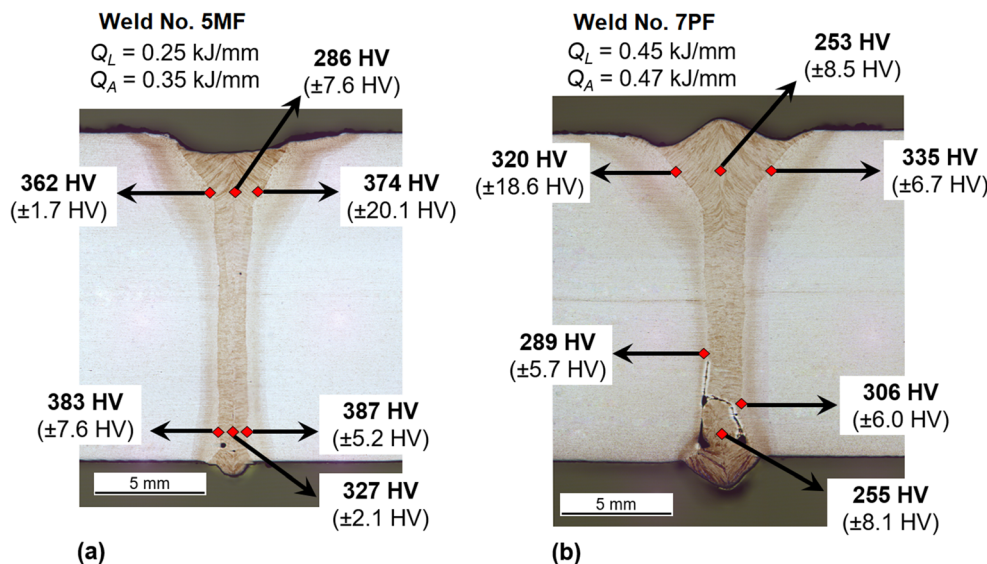


Fig. 17 Microstructure evolution in WM of low (on the left) and high heat input (on the right) experiments in case of 15-mm thick plates. AF—acicular ferrite, PF—polygonal ferrite, LB—lower bainite, LM—lath martensite

Fig. 18 Hardness results in LAHW joints for 15-mm thick plates between low and high heat input: **a** Weld No. 5MF (0.60 kJ/mm) and **b** Weld No. 7PF (0.92 kJ/mm) respectively



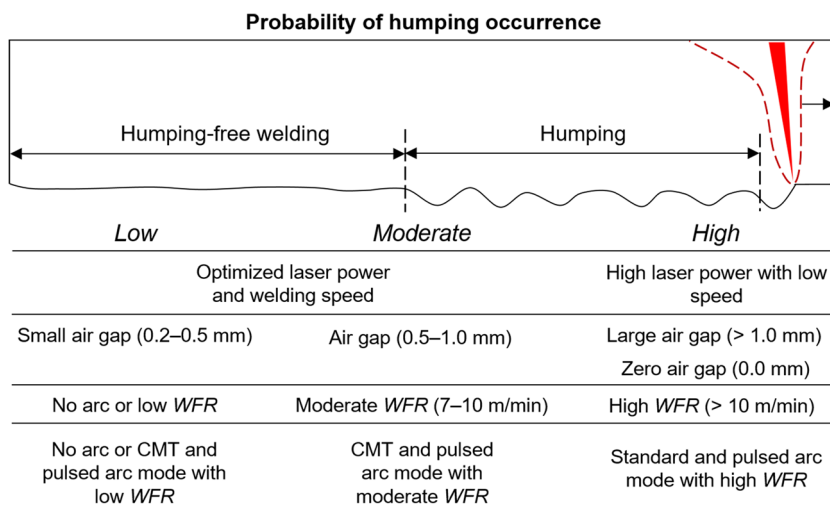
and potentially acceptable parameters are within 14- to 16-kW laser power and 1.1- to 1.5-m/min welding speed ranges combined with limited arc heat input (~0.4 kJ/mm). To achieve acceptable root quality in welding of 15-mm thick plates is very challenging due to complex keyhole physics and conditions. As a result, the process mainly provided incomplete penetration or humping and/or sagging due to severe metal drop-out without a transition phase or humping-free welds with smooth root reinforcement with low height. Plasma cut sidewalls revealed poor suitability for welding. Therefore, machined sidewalls should be used, where the process window is much wider. An increased WFR and arc heat input (as a function of welding speed) significantly affects humping by increasing its probability. So far, the arc mode has not been recognized to influence the humping formation. However, it is possible that pulsed and CMT arc modes are better than the standard arc mode due to better control of metal transfer.

3.2.2 Microstructure and hardness

All welds had high volume fraction of fine-grained AF (> 60%) in the upper area of the WM in case of 15-mm thick plate welding. This is due to the filler wire addition and relatively high combined heat input from laser and arc sources. In the root, some of the welds had a mixture of bainite and lath martensite due to faster cooling rates. Similar results were obtained in previous published work [4].

The microstructure evolution at different depths of welds with low (0.60 kJ/mm) and high (0.92 kJ/mm) heat input is shown in Fig. 17, for Weld No. 5MF and Weld No. 7PF, respectively. For low heat input, a high volume fraction (> 60%) of the fine-grained AF was developed in the top part (the arc dominating part) of the weld, together with PF and some upper bainite. In high heat input weld, a high volume fraction of fine or interlocked AF morphology was developed without bainite. In the root, both welds had AF with elongated grains

Fig. 19 Effect of process parameters of root quality in welding of 12- and 15-mm steel plates



more resembling intragranular ferritic bainite or Widmanstätten ferrite platelets [39, 41, 46, 47] rather than fine-grained AF. Based on these results, it can be clearly seen that filler wire delivery to the root is satisfactory within the selected process parameters. No discoloration (contrast) in the welds was noticed after etching which can reveal that insufficient wire is transported to the root. In CGHAZ, similar microstructure was developed as in LBW welds for 12 mm, a mixture of bainite and some lath martensite with larger prior austenite grains.

The hardness results for LAHW joints are shown in Fig. 18. Low heat input welds provided much higher hardness (> 325 HV) in both WM and HAZ. Welds with high hardness are expected to possess lower toughness, as will be shown later in Section 3.5. According to DNVGL-OS-C401 standard [48], maximum acceptable hardness is 325 HV. However, this standard does not include laser or laser hybrid welding.

Based on this upper HV limit, welds with heat input (> 0.80–0.90 kJ/mm) may be qualified. The hardness results are in a good agreement with the microstructure observations.

3.3 Humping mechanism

Humping in the root area was the main welding defect observed in joining of 12- and 15-mm thick plates. Based on the experimental observations, there are a few determining factors affecting the humping phenomenon. A summary on how process parameters affect humping is presented in Fig. 19. A slight air gap can be beneficial for suppressing humping by reduction of the pressure in the keyhole. However, larger air gap exceeding a critical size will cause humping or sagging of the melt since the surface tension is not capable to sustain the dropout. Moreover, in deep penetration welding molten metal velocities can reach > 15 m/s at the front wall of the keyhole [49, 50], depending on the process parameters. Therefore, during full penetration the molten metal flow at high speeds

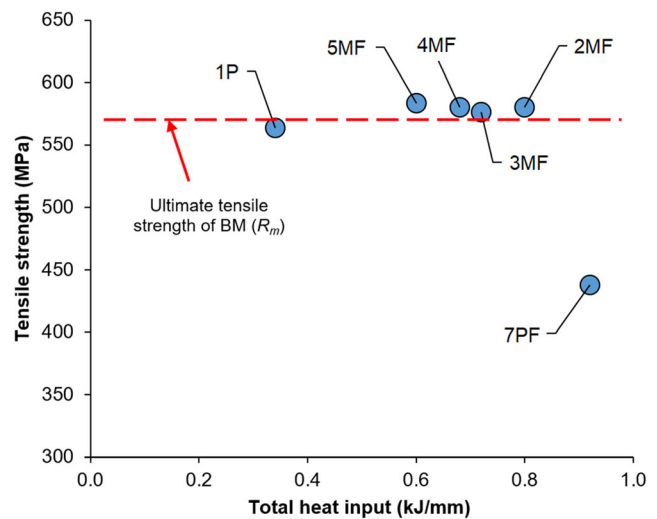
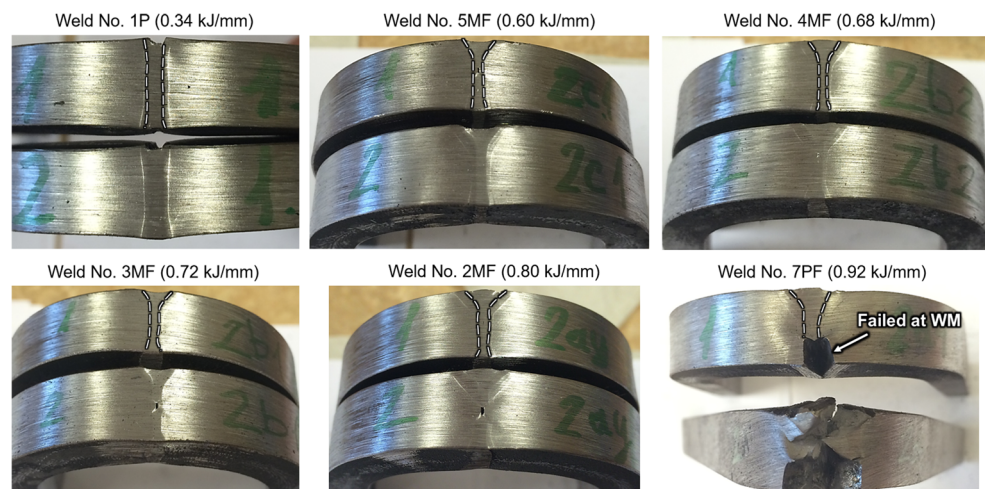


Fig. 21 Effect of total heat input on cross-weld tensile strength

requires substantial surface tension or strong forces for redirection [10] to prevent humping/sagging. The added arc increases the humping probability. Thus, a lower WFR should be used to reduce mass momentum in the weld pool, together with a more controlled droplet transfer mode such as CMT or pulsed arc. Another important factor is the sensitive balance between laser power and welding speed which requires optimization to suppress humping effectively.

Comprehensive and reliable studies of pressure inside the keyhole and its effect on the melt flow have not been published. This may be related to challenges in process observations and measurements related to high temperatures and evaporation phenomena [51]. During keyhole welding, high laser beam power causes high temperatures and evaporation rates resulting in strong recoil or dynamics pressure [52]. Possibly, the recoil pressure is not so high to cause the most determining factor on melt flows [53]. In fact, evaporation of metal is low during laser keyhole welding. However, it is evident that by increasing the laser beam power, a higher

Fig. 20 Bending test results. WM geometry indicated by dashed lines



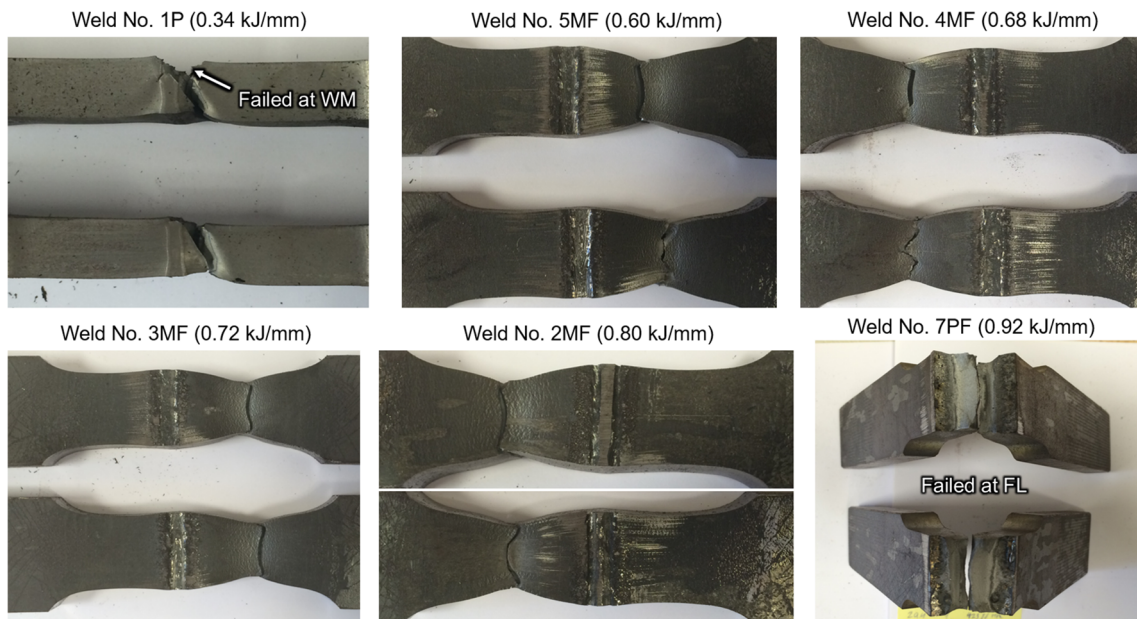


Fig. 22 Visual inspection of tensile test specimens

pressure with an associated expulsion of molten metal in form of ejections is present based on experimental trials. Accordingly, the change of unfavorable melt flow dynamics can be a significant factor in formation of humping. To study melt flow under such conditions is very complicated requiring X-ray filmography and tracking particles (such as tungsten). Moreover, it requires advanced equipment for analysis [54]. Evidently, with an increase of plate thickness from 12 to 15 mm, the frequency of humping occurrence is higher due to an increased molten mass of the weld pool. It was shown that duplex stainless steels having very different chemical composition provides much less humping [55]. Pan et al. [56] showed that the use of CO₂ in the shielding gas significantly increased the process window, which may be attributed to the change of molten metal chemistry and physical properties such as surface tension. As a result, the surface tension can be another significant factor as described in literature [10, 57].

In summary, the formation of high-quality root without humping in joining thick plates (12–15 mm) with high power laser beams is a delicate balance involving several factors:

- Balance of pressure inside the keyhole pushing molten metal downwards and surface tension to keep the molten metal;
- Keyhole stability (physical state and parameters, e.g., recoil pressure);
- Melt flow dynamics (direction and velocity) and effect of external forces (from the arc) when LAHW is used;
- Surface tension conditions depending on the chemical composition of the steel, the shielding gas and the filler wire when LAHW is used;
- Machined sidewalls provide better and more consistent root quality due to high degree of transverse flatness and perpendicularity.

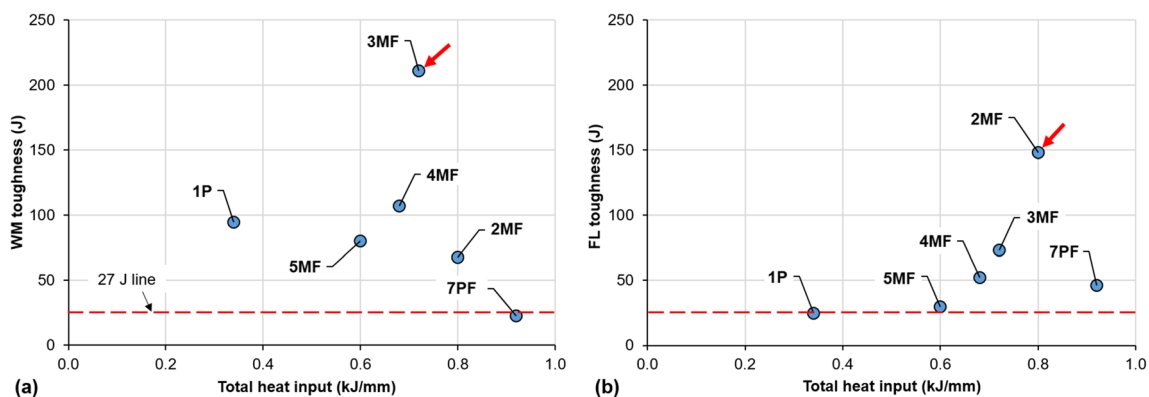


Fig. 23 Average Charpy V-notch toughness of butt joints at $-50\text{ }^{\circ}\text{C}$ with notch positioned in **a** weld metal and **b** fusion line

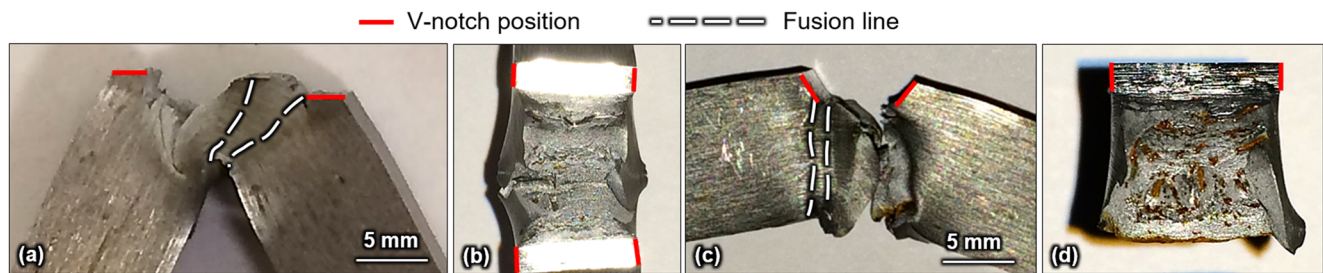


Fig. 24 Charpy V-notch specimens after fracture at $-50\text{ }^{\circ}\text{C}$ environment: **a, b** Weld No. 3MF and **c, d** Weld No. 2MF

There are still many undiscovered parameters and laser characteristics left to study concerning their effects on root quality in single-pass single-sided welds on thick plates. Some parameters can strongly affect melt flow and its parameters such as focal point position [58], polarization [59], beam caustics related to lateral power density distribution [60], complex laser and arc beam interactions in case of LAHW [61], and surface quality.

3.4 Mechanical test results

Qualitative results of bend test are shown in Fig. 20. All welds, except Weld No. 7PF (with the highest heat input of 0.92 kJ/mm), passed the bending test even though some cracking was visible mainly in the WM center.

Most welds showed good tensile strength exceeding the strength of the base metal (which was 570 MPa), resulting in failure in the BM. The effect of heat input on tensile strength is shown in Fig. 21. Generally, the tensile strength is reduced with increasing heat input due to internal imperfections (porosity) and microstructure and might due to larger grains providing lower strength [62]. Weld No. 1P had a failure started in the WM (crack propagated to HAZ) mainly due to underfill acting as a stress concentrator in combination with higher cooling rates resulting in high hardness. For the highest heat input sample (Weld No. 7PF), a visual inspection revealed the existence of porosity in the WM (Fig. 22) and lack of fusion with sidewalls visible in Fig. 18b. Thus, LBW and LAHW provide acceptable tensile strength in a wide range of heat inputs when no weld imperfections are present.

The Charpy test results with the notch in WM are presented in Fig. 23a. All welds, except Weld No. 7PF, provided high toughness ($> 50\text{ J}$ at $-50\text{ }^{\circ}\text{C}$). One of the welds had particularly high toughness (Weld No. 3MF, $> 200\text{ J}$) which is possibly due to the fracture deviation into the fine-grained HAZ (FGHAZ) and the BM (Fig. 24a). Based on the results achieved, the preferable heat input for WM lies within the range of 0.6–0.8 kJ/mm.

The toughness results for the fusion line (FL) position (see Fig. 23b) showed lower toughness than for the WM position due to the formation of brittle bainite microstructure in the HAZ. For FL samples, higher toughness was achieved with

increasing heat input. As a result, higher heat input seems positive for the FL toughness. This observation is possibly linked to softer microstructures that develop during slower cooling rates. Higher heat input will reduce the amount of hard lath martensite in favor of the upper bainite in the HAZ as well as alteration in morphology [63, 64]. As a result, higher heat input within the employed parameter range appears to be positive for the FL toughness. This trend was also partly observed in previous work in welding of 45-mm thick high strength steel [4]. However, excessively high heat input ($< 2.0\text{ kJ/mm}$) is proven to be detrimental for HAZ toughness [65] mainly due to very large grains and unfavorable crystallographic features [66, 67].

High toughness was achieved in case of Weld No. 2MF since cracking deviated into the FGHAZ and the BM (Fig. 24b). On the contrary, the lowest values were always associated with crack propagation along the FL. In cases with very high impact toughness, a clear evidence of high plastic deformation is visible by the characteristic large shear lips for WM specimen and FL specimen, Fig. 24c and Fig. 24d respectively.

In summary, the highest toughness at FL was achieved within the heat input range of 0.6–0.8 kJ/mm. Thus, this heat input range is apparently the optimum for both the weld metal and the fusion line positions. Finally, the same optimum heat input was also found for the cross-weld tensile strength with fracture in the base metal.

4 Conclusions

Based on the present experimental results the following conclusions can be drawn:

- Laser-arc hybrid welding is susceptible to root humping due to unfavorable melt flow at the bottom of the weld pool. Wide fusion zone width in the root causes dropouts and sagging.
- Humping-free welds can be made within a narrow process window with a certain combination between laser beam and arc power, as well as welding speed.
- Slower welding speed ($< 1.2\text{ m/min}$) and lower laser beam power ($< 14\text{ kW}$) provide more stable keyhole processing

and thus humping can be reduced or at least provide safer welding conditions.

- The process window is much wider for machined sidewalls compared with plasma cut sidewalls.
- High amount of acicular ferrite was formed in the weld metal within a wide range of employed process parameters showing versatility and good filler wire mixing in laser-arc hybrid welding in 12- to 15-mm thickness of the plates.
- High toughness was achieved at $-50\text{ }^{\circ}\text{C}$ within a wide range of heat inputs (0.34–0.92 kJ/mm) showing high viability of the autogenous laser beam and the laser-arc hybrid welding processes for steel containing up to 0.14 wt.% C.

Acknowledgments The authors acknowledge FORCE Technology (Denmark) and SSAB (Finland) for kind cooperation. Dr. Sergio Armada Nieto, SINTEF, is appreciated for roughness and surface morphology data.

Funding information Open Access funding provided by SINTEF AS. The authors wish to thank the Statens vegvesen AS (Norway) for funding the project.

Open Access This article is licensed under a Creative Commons Attribution 4.0 International License, which permits use, sharing, adaptation, distribution and reproduction in any medium or format, as long as you give appropriate credit to the original author(s) and the source, provide a link to the Creative Commons licence, and indicate if changes were made. The images or other third party material in this article are included in the article's Creative Commons licence, unless indicated otherwise in a credit line to the material. If material is not included in the article's Creative Commons licence and your intended use is not permitted by statutory regulation or exceeds the permitted use, you will need to obtain permission directly from the copyright holder. To view a copy of this licence, visit <http://creativecommons.org/licenses/by/4.0/>.

References

1. Webster S, Kristensen JK, Petring D (2008) Joining of thick section steels using hybrid laser welding. *Ironmak Steelmak* 35(7):496–504. <https://doi.org/10.1179/174328108X358505>
2. Sokolov M, Salminen A, Kuznetsov M, Tsibulskiy I (2011) Laser welding and weld hardness analysis of thick section S355 structural steel. *Mater Des* 32(10):5127–5131. <https://doi.org/10.1016/j.matdes.2011.05.053>
3. Gook S, Gumenyuk A, Rethmeier M (2014) Hybrid laser arc welding of X80 and X120 steel grade. *Sci Technol Weld Join* 19(1):15–24. <https://doi.org/10.1179/1362171813Y.0000000154>
4. Bunaziv I, Akselsen OM, Frostevarg J, Kaplan AFH (2018d) Deep penetration fiber laser-arc hybrid welding of thick HSLA steel. *J Mater Process Technol* 256:216–228. <https://doi.org/10.1016/j.jmatprotec.2018.02.026>
5. Turichin G, Kuznetsov M, Pozdnyakov A, Gook S, Gumenyuk A, Rethmeier M (2018) Influence of heat input and preheating on the cooling rate, microstructure and mechanical properties at the hybrid laser-arc welding of API 5L X80 steel. *Procedia CIRP* 74:748–751. <https://doi.org/10.1016/j.procir.2018.08.018>
6. Bunaziv I, Akselsen OM, Frostevarg J, Kaplan AFH (2019) Application of laser-arc hybrid welding of steel for low-temperature service. *Int J Adv Manuf Technol* 102(5):2601–2613. <https://doi.org/10.1007/s00170-019-03304-1>
7. Vollertsen F, Gruenenwald S Defects and process tolerances in welding of thick plates. In: 27th International Congress on Applications of Lasers and Electro-Optics (ICALEO), Temecula, California, USA, October 20-23rd 2008. Laser Institute of America, pp 489–497
8. Reutzel EW, Kelly SM, Sullivan MJ, Huang TD, Kvidahl L, Martukanitz RP (2008) Hybrid laser-GMA welding for improved affordability. *J Ship Prod* 24(2):72–81
9. Haug P, Rominger V, Speker N, Weber R, Graf T, Weigl M, Schmidt M (2013) Influence of laser wavelength on melt bath dynamics and resulting seam quality at welding of thick plates. *Phys Procedia* 41:49–58. <https://doi.org/10.1016/j.phpro.2013.03.051>
10. Frostevarg J (2018) Factors affecting weld root morphology in laser keyhole welding. *Opt Lasers Eng* 101(supplement C):89–98. <https://doi.org/10.1016/j.optlaseng.2017.10.005>
11. Avilov V, Fritzsche A, Bachmann M, Gumenyuk A, Rethmeier M (2016) Full penetration laser beam welding of thick duplex steel plates with electromagnetic weld pool support. 28(2):022420. <https://doi.org/10.2351/1.4944103>
12. Bachmann M, Avilov V, Gumenyuk A, Rethmeier M (2014) Experimental and numerical investigation of an electromagnetic weld pool support system for high power laser beam welding of austenitic stainless steel. *J Mater Process Technol* 214(3):578–591. <https://doi.org/10.1016/j.jmatprotec.2013.11.013>
13. Fritzsche A, Avilov V, Gumenyuk A, Hilgenberg K, Rethmeier M (2016) High power laser beam welding of thick-walled ferromagnetic steels with electromagnetic weld pool support. *Phys Procedia* 83:362–372. <https://doi.org/10.1016/j.phpro.2016.08.038>
14. Qi Y, Chen G (2018) Root defects in full penetration laser welding of thick plates using steady electromagnetic force. *J Mater Process Technol* 260:97–103. <https://doi.org/10.1016/j.jmatprotec.2018.05.009>
15. Qi Y, Chen G, Deng S, Zhou D (2019) Periodic root humps in thick-plate laser welding using steady electromagnetic force. *J Mater Process Technol* 273:116247. <https://doi.org/10.1016/j.jmatprotec.2019.05.028>
16. Üstündağ Ö, Gook S, Gumenyuk A, Rethmeier M (2020) Hybrid laser arc welding of thick high-strength pipeline steels of grade X120 with adapted heat input. *J Mater Process Technol* 275:116358. <https://doi.org/10.1016/j.jmatprotec.2019.11.6358>
17. Weberpals J-P, Krueger P, Berger P, Graf T. Understanding the influence of the focal position in laser welding on spatter reduction. In: 30th International Congress on Applications of Lasers and Electro-Optics (ICALEO), Orlando, Florida, USA, October 23-27th 2011. Laser Institute of America, pp 159–168
18. Frostevarg J, Qinglong P, Mizutani M, Kawahito Y, Katayama S (2018) Effects of edge oxides from laser cutting in laser-arc hybrid welding. *J Laser Appl* 30(1):012014. <https://doi.org/10.2351/1.5009792>
19. Sokolov M, Salminen A, Somonov V, Kaplan AFH (2012) Laser welding of structural steels: influence of the edge roughness level. *Opt Laser Technol* 44(7):2064–2071. <https://doi.org/10.1016/j.optlastec.2012.03.025>
20. Lacroix D, Jeandel G, Boudot C (1998) Solution of the radiative transfer equation in an absorbing and scattering Nd:YAG laser-induced plume. *J Appl Phys* 84(5):2443–2449. <https://doi.org/10.1063/1.368405>
21. Matsunawa A, Ohnawa T (1991) Beam-plume interaction in laser materials processing. *Trans JWRI* 21(1):9–15
22. Shcheglov PY, Gumenyuk AV, Gornushkin IB, Rethmeier M, Petrovskiy VN (2013) Vapor-plasma plume investigation during high-power fiber laser welding. *Laser Phys* 23(1). <https://doi.org/10.1088/1054-660X/23/1/016001>

23. Shcheglov PY, Uspenskiy SA, Gumenyuk AV, Petrovskiy VN, Rethmeier M, Yermachenko VM (2011) Plume attenuation of laser radiation during high power fiber laser welding. *Laser Phys Lett* 8(6):475
24. Steen WM, Mazumder J (2010) *Laser material processing*. Springer
25. Bunaziv I, Frostevarg J, Akselsen OM, Kaplan AFH (2018a) Process stability during fiber laser-arc hybrid welding of thick steel plates. *Opt Lasers Eng* 102(supplement C):34–44. <https://doi.org/10.1016/j.optlaseng.2017.10.020>
26. Frostevarg J (2016) Comparison of three different arc modes for laser-arc hybrid welding steel. *J Laser Appl* 28:022407. <https://doi.org/10.2351/1.4944098>
27. ISO 5173 - Destructive tests on welds in metallic materials - Bend tests (2009) International Organization for Standardization
28. EN ISO 4136 - Destructive tests on welds in metallic materials - Transverse tensile test (2013) International Organization for Standardization
29. ISO 9016 - Destructive tests on welds in metallic materials - Impact tests - Test specimen location, notch orientation and examination (2012) International Organization for Standardization
30. ISO 17639 - Destructive tests on welds in metallic materials - Macroscopic and microscopic examination of welds (2003) International Organization for Standardization
31. ISO 22826 - Destructive tests on welds in metallic materials - Hardness testing of narrow joints welded by laser and electron beam (Vickers and Knoop hardness tests) (2005) International Organization for Standardization
32. ISO 13919-1 - Welding - electron and laser-beam welded joints - guidance on quality levels for imperfections - Part 1: Steel (1996) International Organization for Standardization
33. Bunaziv I, Akselsen OM, Ren X, Salminen A (2015) Hybrid welding possibilities of thick sections for Arctic applications. *Phys Procedia* 78(supplement C):74–83. <https://doi.org/10.1016/j.phpro.2015.11.019>
34. ISO 12932 - Welding - laser-arc hybrid welding of steels, nickel and nickel alloys - quality levels for imperfections (2013) International Organization for Standardization
35. Lancaster JF (1986) *The physics of welding*, 2nd edn. Pergamon Press
36. Eriksson I, Powell J, Kaplan AFH (2014) Surface tension generated defects in full penetration laser keyhole welding. *26(1):012006*. <https://doi.org/10.2351/1.4830175>
37. Cho W-I, Schultz V, Woizeschke P (2018) Numerical study of the effect of the oscillation frequency in buttonhole welding. *J Mater Process Technol* 261:202–212. <https://doi.org/10.1016/j.jmatprotec.2018.05.024>
38. Tang G, Zhao X, Li R, Liang Y, Jiang Y, Chen H (2020) The effect of arc position on laser-arc hybrid welding of 12-mm-thick high strength bainitic steel. *Opt Laser Technol* 121:105780. <https://doi.org/10.1016/j.optlastec.2019.105780>
39. Zhang D, Terasaki H, Yi K (2010) In situ observation of the formation of intragranular acicular ferrite at non-metallic inclusions in C–Mn steel. *Acta Mater* 58(4):1369–1378. <https://doi.org/10.1016/j.actamat.2009.10.043>
40. Díaz-Fuentes M, Iza-Mendia A, Gutiérrez I (2003) Analysis of different acicular ferrite microstructures in low-carbon steels by electron backscattered diffraction. Study of their toughness behavior. *Metall Mater Trans A* 34(11):2505–2516. <https://doi.org/10.1007/s11661-003-0010-7>
41. Ricks RA, Howell PR, Barritte GS (1982) The nature of acicular ferrite in HSLA steel weld metals. *J Mater Sci* 17(3):732–740. <https://doi.org/10.1007/bf00540369>
42. Bhadeshia HKDH, Honeycombe RWK (2006) *Steels: microstructure and properties*, 3rd edn. Butterworth-Heinemann
43. Coelho RS, Corpas M, Moreto JA, Jahn A, Standfuß J, Kaysser-Pyzalla A, Pinto H (2013) Induction-assisted laser beam welding of a thermomechanically rolled HSLA S500MC steel: a microstructure and residual stress assessment. *Mater Sci Eng A* 578(supplement C):125–133. <https://doi.org/10.1016/j.msea.2013.04.039>
44. Jahn A, Krätzsich M (2008) Brenner B induction assisted laser beam welding of HSLA steel sheets. In: *International scientific colloquium modelling for electromagnetic processing*. Univ. Hannover, Hannover, pp 195–200
45. Ilar T, Eriksson I, Powell J, Kaplan A (2012) Root humping in laser welding – an investigation based on high speed imaging. *Phys Procedia* 39(0):27–32. <https://doi.org/10.1016/j.phpro.2012.10.010>
46. Shim JH, Cho YW, Chung SH, Shim JD, Lee DN (1999) Nucleation of intragranular ferrite at Ti₂O₃ particle in low carbon steel. *Acta Mater* 47(9):2751–2760. [https://doi.org/10.1016/S1359-6454\(99\)00114-7](https://doi.org/10.1016/S1359-6454(99)00114-7)
47. Babu SS (2004) The mechanism of acicular ferrite in weld deposits. *Curr Opin Solid State Mater Sci* 8(3):267–278. <https://doi.org/10.1016/j.cossms.2004.10.001>
48. DNVGL-OS-C401: Fabrication and testing of offshore structures (July 2015). DNV GL AS
49. Eriksson I, Powell J, Kaplan AFH (2011) Measurements of fluid flow on keyhole front during laser welding. *Sci Technol Weld Join* 16(7):636–641. <https://doi.org/10.1179/1362171811Y.00000000050>
50. Eriksson I, Powell J, Kaplan AFH (2013) Melt behavior on the keyhole front during high speed laser welding. *Opt Lasers Eng* 51(6):735–740. <https://doi.org/10.1016/j.optlaseng.2013.01.008>
51. Le-Quang T, Shevchik SA, Meylan B, Vakili-Farahani F, Olbinado MP, Rack A, Wasmer K (2018) Why is in situ quality control of laser keyhole welding a real challenge? *Procedia CIRP* 74:649–653. <https://doi.org/10.1016/j.procir.2018.08.055>
52. Tenner F, Brock C, Gürtler F-J, Klämpfl F, Schmidt M (2014) Experimental and numerical analysis of gas dynamics in the keyhole during laser metal welding. *Phys Procedia* 56:1268–1276. <https://doi.org/10.1016/j.phpro.2014.08.050>
53. Seidgazov RD (2009) Thermocapillary mechanism of melt displacement during keyhole formation by the laser beam. *J Phys D Appl Phys* 42(17):175501. <https://doi.org/10.1088/0022-3727/42/17/175501>
54. Aucott L, Dong H, Mirihanage W, Atwood R, Kidess A, Gao S, Wen S, Marsden J, Feng S, Tong M, Connolly T, Drakopoulos M, Kleijn CR, Richardson IM, Browne DJ, Mathiesen RH, Atkinson HV (2018) Revealing internal flow behaviour in arc welding and additive manufacturing of metals. *Nat Commun* 9(1):5414. <https://doi.org/10.1038/s41467-018-07900-9>
55. Rominger V, Haug P, Speker N, Holzer M (2013) High-power full penetration welding behavior. *Laser Tech J* 10(3):36–40
56. Pan Q, Mizutani M, Kawahito Y, Katayama S (2016) Effect of shielding gas on laser–MAG arc hybrid welding results of thick high-tensile-strength steel plates. *Weld World* 60(4):653–664. <https://doi.org/10.1007/s40194-016-0333-9>
57. Blecher JJ, Palmer T, DebRoy T (2015) Mitigation of root defect in laser and hybrid laser-arc welding. *Weld J* 94:73–82
58. Schaefer M, Kessler S, Fetzner F, Graf T (2017) Influence of the focal position on the melt flow during laser welding of steel. *J Laser Appl* 29(1):012010. <https://doi.org/10.2351/1.4972098>
59. Weber R, Michalowski A, Abdou-Ahmed M, Onuseit V, Rominger V, Kraus M, Graf T (2011) Effects of radial and tangential polarization in laser material processing. *Phys Procedia* 12:21–30. <https://doi.org/10.1016/j.phpro.2011.03.004>
60. Kaplan AFH (2011) Modelling the primary impact of an Yb:fibre laser beam profile on the keyhole front. *Phys Procedia* 12(part a (0)):627–637. <https://doi.org/10.1016/j.phpro.2011.03.079>
61. Mu Z, Chen X, Zheng Z, Huang A, Pang S (2019) Laser cooling arc plasma effect in laser-arc hybrid welding of 316L stainless steel. *Int J Heat Mass Transf* 132:861–870. <https://doi.org/10.1016/j.ijheatmasstransfer.2018.12.050>

62. Zhou Y, Jia T, Zhang X, Liu Z, Misra RDK (2015) Microstructure and toughness of the CGHAZ of an offshore platform steel. *J Mater Process Technol* 219(supplement C):314–320. <https://doi.org/10.1016/j.jmatprotec.2014.12.017>
63. Lambert-Perlade A, Sturel T, Gourgues AF, Besson J, Pineau A (2004) Mechanisms and modeling of cleavage fracture in simulated heat-affected zone microstructures of a high-strength low alloy steel. *Metall Mater Trans A* 35(3):1039–1053. <https://doi.org/10.1007/s11661-004-0030-y>
64. Lambert A, Lambert A, Drillet J, Gourgues AF, Sturel T, Pineau A (2000) Microstructure of martensite–austenite constituents in heat affected zones of high strength low alloy steel welds in relation to toughness properties. *Sci Technol Weld Join* 5(3):168–173. <https://doi.org/10.1179/136217100101538164>
65. Cao R, Li J, Liu DS, Ma JY, Chen JHJM (2015) Micromechanism of decrease of impact toughness in coarse-grain heat-affected zone of hsla steel with increasing welding heat input. *Metall Mater Trans A* 46(7):2999–3014. <https://doi.org/10.1007/s11661-015-2916-2>
66. Lan L, Kong X, Qiu C, Zhao D (2016) Influence of microstructural aspects on impact toughness of multi-pass submerged arc welded HSLA steel joints. *Mater Des* 90(supplement C):488–498. <https://doi.org/10.1016/j.matdes.2015.10.158>
67. Wang XL, Wang ZQ, Dong LL, Shang CJ, Ma XP, Subramanian SV (2017) New insights into the mechanism of cooling rate on the impact toughness of coarse grained heat affected zone from the aspect of variant selection. *Mater Sci Eng A* 704(supplement C): 448–458. <https://doi.org/10.1016/j.msea.2017.07.095>

Publisher's note Springer Nature remains neutral with regard to jurisdictional claims in published maps and institutional affiliations.